Title

Histology of type 3 macular neovascularization and microvascular anomalies in anti-VEGF treated age-related macular degeneration

Authors

Andreas Berlin MD MS,[1,2] Diogo Cabral MD,[3,4] Ling Chen, MD PhD,[1,5] Jeffrey D Messinger DC,[1] Chandrakumar Balaratnasingam MD PhD,[6-8] Randev Mendis MD,[9] Daniela Ferrara MD PhD,[10] K. Bailey Freund MD,[3,11] Christine A Curcio PhD[1]*

[1] Department of Ophthalmology and Visual Sciences, School of Medicine, University of Alabama at Birmingham, Birmingham AL, USA; [2] Department of Ophthalmology, University Hospital Wu□rzburg, Wu□rzburg, Germany; [3] Vitreous Retina Macula Consultants of New York NY, USA; [4] NOVA Medical School Research, Universidade NOVA de Lisboa, Portugal; [5] The First Affiliated Hospital of Chongqing Medical University, Chongqing Key Laboratory of Ophthalmology, and Chongqing Eye Institute, Chongqing, China; [6] Centre for Ophthalmology and Visual Science, University of Western Australia, Perth, Australia; [7] Lions Eye Institute, Nedlands, Western Australia, Australia; [8] Department of Ophthalmology, Sir Charles Gairdner Hospital, Western Australia, Australia; [9] Canberra Retina Center, Canberra Australia, [10] Genentech, South San Francisco, CA, USA; [11] Department of Ophthalmology, New York University Grossman School of Medicine, New York NY, USA

*Corresponding author

Short title Intraretinal vascular morphologies in treated AMD

Word count 4147

Figures 11

Tables 1

Supplementary 3 figures, 1 video, 1 table

Corresponding Address

Christine A. Curcio, PhD; Department of Ophthalmology and Visual Sciences; EyeSight Foundation of Alabama Vision Research Laboratories; 1670 University Boulevard Room 360; University of Alabama at Birmingham, School of Medicine; Birmingham AL 35294-0099; Email: christinecurcio@uabmc.edu

Key words

age-related macular degeneration, type 3 macular neovascularization, deep retinal age-related microvascular anomalies, vascular morphology, optical coherence tomography angiography, histopathology, electron microscopy.

Abstract

Objective/Purpose

Correlation of in vivo multimodal imaging of intraretinal neovascularization and microvascular anomalies with corresponding ex vivo histology.

Design

Case study, clinical imaging from a community-based practice, and histologic analysis at a university-based research laboratory (clinicopathologic correlation).

Participants

A white woman in her 90's treated with numerous intravitreal anti-vascular endothelial growth factor (VEGF) injections for bilateral type 3 macular neovascularization (MNV) secondary to age-related macular degeneration (AMD).

Intervention(s)/ Methods

Infrared reflectance, eye-tracked spectral-domain optical coherence tomography (OCT), OCT angiography, and fluorescein angiography were correlated via eye tracking with ex vivo high-resolution histology and electron microscopy of the preserved donor eyes.

Main Outcome(s) and Measure(s)

Histologic descriptions of vessels seen in clinical imaging.

Results

By histology of both eyes, 7 vascular lesions were confirmed within 500-1520 µm from the foveal center. These included three type 3 MNV lesions traversing the retinal pigment epithelium (RPE) and four deep retinal age-related microvascular anomalies (DRAMA) located anterior to the outer nuclear layer. Type 3 MNV morphologies included both a vertically oriented, pyramidal structure and a horizontally oriented, tangled configuration. Both phenotypes originated at the level of the deep capillary plexus and dove posteriorly, without extension below sub-RPE basal laminar deposit, or receiving contributions from choroidal vessels. Neovascular complexes contained capillaries with

dilated lumens, non-fenestrated endothelial cells, and pericytes. Vessels were associated with RPE transdifferentiation, anterior migration, and atrophy. The four DRAMA lesions sagged into the Henle fiber layer. One of these lesions was encircled by a tower of RPE cells that was continuous with an intact RPE layer and lacked external limiting membrane descents signifying atrophy. External and internal diameters of type 3 MNV and DRAMA vessels were larger than comparison vessels in the index eyes, intermediate AMD eyes, and control eyes.

Conclusions

Type 3 MNV exhibits different morphologies, reflects specializations of source capillaries, and persists during anti-VEGF therapy. Especially for neovessels with collagenous sheaths, flow signal detection via OCTA may assist treatment decisions. Further investigation with longitudinal imaging before exudation onset will help determine the relation of DRAMA to type 3 MNV progression.

Precis

In fellow eyes with anti-vascular endothelial growth factor-treated AMD, clinicopathologic correlation reveals type 3 macular neovascularization with endothelial specializations like deep capillary plexus. Some vessels sag into Henle fiber layer, resembling deep retinal age-related microvascular anomalies.

Abbreviations

AMD, age-related macular degeneration; BLamD, basal laminar deposit; BrM, Bruch's membrane; ChC, choriocapillaris; Ch, choroid; DCP, deep capillary plexus; DRAMA, deep retinal age-related microvascular anomaly; ELM, external limiting membrane; FA, fluorescein angiography; GCL, ganglion cell layer; HFL, Henle fiber layer; ICP,

intermediate capillary plexus; INL, inner nuclear layer; IPL, inner plexiform layer; IS, inner segment; MNV, macular neovascularization; nvAMD, neovascular age-related macular degeneration; OCT, optical coherence tomography; OCTA, optical coherence tomography angiography; ONL, outer nuclear layer; OPL, outer plexiform layer; OS, outer segment; RPE, retinal pigment epithelium; SPC, superficial capillary plexus.

Introduction

Type 3 macular neovascularization (type 3 MNV) is a subtype of neovascular age-related macular degeneration (AMD).[1] Unlike type 1 arising from the choroid, type 3 MNV originates in the neurosensory retina.[2-4] Female gender, older age, and presence of subretinal drusenoid deposits confer risk for type 3 MNV.[5, 6] Among patients of European descent presenting with unilateral neovascular AMD, type 3 MNV occurs in up to 1/3.[7] Fellow eyes often convert to neovascular AMD within 3 years.[8-10] Early lesions respond well to intravitreal anti-vascular endothelial growth factor (VEGF) therapy, unlike chronic lesions.[3, 11]

Recent clinical imaging studies have elucidated type 3 MNV pathophysiology. Stages have been defined based on structural optical coherence tomography (OCT). Precursors to Stage 1 are hyperreflective foci at the level of the deep capillary plexus (DCP), often near drusen. Stage 1 includes an intraretinal hyperreflective lesion and cystoid macular edema. In Stage 2, outer retinal disruption appears. At Stage 3, the hyperreflective lesion extends into the sub-RPE basal lamina (BL) space, associated with a pigment epithelium detachment.[3] By color fundus photography, fluorescein angiography (FA), and OCT, type 3 MNV exhibit a specific regional distribution and pattern of hemorrhage.[12-14] Lesions localize preferentially to the inner ring of the Early Treatment of Diabetic Retinopathy Study (ETDRS) grid. Flame-shaped intraretinal hemorrhages are located over type 3 MNV lesions, pointing toward the fovea. Optical coherence tomography angiography (OCTA) with 3-dimensional reconstruction and display is useful for viewing in vivo the vertically oriented components of type 3 MNV. Using this technology, Borelli et al described two morphologic phenotypes (‘filiform’ and ‘saccular’) of advanced type 3 MNV.[15]

Through clinicopathological correlation, the morphology of type 3 neovascular complexes, associated cell types, and contents of the sub-RPE-BL space corresponding

to OCT-based stages have been elucidated.[16, 17] Vertically oriented vascular complexes shaped like base-down pyramids were described.[4, 17] Vessels surrounded by collagenous material originated at the DCP, expanded posteriorly, and crossed persistent basal laminar deposit (BLamD) to enter the sub-RPE-BL space. Macrophages, VEGF-positive fibroblasts, lymphocytes, Müller cell processes, and subducted RPE cells were identified.[12, 13] Hence, ischemia and inflammatory pathways were suggested in the development and progression of type 3 MNV.[12, 13]

Descriptions of microvascular abnormalities involving the DCP include microaneurysms, telangiectasia, perifoveal exudative anomalous vascular complex (PEVAC), and capillary macroaneurysms. [18-23] PEVAC was initially described in non-AMD eyes as an isolated aneurysmal dilation of a retinal capillary originating between the superficial and deep plexuses, with exudation that was unresponsive to intravitreal anti-VEGF therapy.[18, 23, 24] Deep retinal age-related microvascular anomalies (DRAMA) were recently proposed to describe DCP alterations in the setting of AMD findings including soft drusen and intraretinal hyperreflective foci. Eyes with DRAMA show abnormal horizontal or vertical vessels with a diameter of >50 µm and/or a location below the posterior border of the outer plexiform layer (OPL) .[25] In contrast to type 1 MNV,[26] precursors, early stages, and potential masqueraders for type 3 MNV have not been described at the histologic level.[27] Such information if available could support improved detection and treatment decisions in affected patients. Histological analysis of human eyes with longitudinal clinical imaging are especially valuable for this purpose.[4]

Herein we directly compared longitudinal OCT and angiographic signatures of intraretinal neovascularization and microvascular anomalies to corresponding histology in two eyes of a patient who received intravitreal anti-VEGF treatments for type 3 MNV over the course of 5 years (right eye) and 9 months (left eye).

149

Methods

Compliance

Approval for this study was obtained by Institutional review at the University of Alabama at Birmingham (protocol #300004907). The study was conducted in accordance with the tenets of the Declaration of Helsinki and the Health Insurance Portability and Accountability Act of 1996.[28, 29]

Clinical course

A white, pseudophakic woman in her 90's received comprehensive ophthalmologic examination and multimodal imaging during a 5-year follow-up for bilateral type 3 MNV secondary to AMD. The patient presented in 2014 with exudative type 3 MNV in the right eye. Over 5 years, she received a total of 37 intravitreal anti-VEGF injections over approximately 6 fluid resorption cycles in the right eye (12 x 0.5 mg/ 0.05 ml ranibizumab then 25 x 2 mg/ 0.05 ml aflibercept). The left eye was diagnosed with exudative type 3 MNV 4 years after the right eye. Over 9 months, the left eye received a total of 6 intravitreal anti-VEGF injections over approximately 2 fluid resorption cycles (12 x 0.5 mg/ 0.05 ml ranibizumab). Her general medical history included dyslipidemia as well as paroxysmal atrial fibrillation. In late 2018, the patient was diagnosed with gallbladder adenocarcinoma. Her last ophthalmic evaluation and anti-VEGF treatment of the right eye was in January 2019, 2 months before death due to adenocarcinoma.

Clinical image capture and analysis

All images were acquired using Spectralis HRA+OCT (Heidelberg Engineering, Heidelberg, Germany). Available for review were 11 (right eye) and 7 (left eye) eye-tracked spectral domain OCT volumes (6 mm x 6 mm horizontal and radial scans; 20° x 20° field) and FA at first presentation and 4 years later.

One eye-tracked spectral domain OCTA volume (3 mm x 3 mm horizontal scans, 256 B-scans at 6 µm spacing, 10° x 10° field, ART 5, quality 34 dB) was obtained of the

right eye 3.5 years after presentation in 2017. Seven repeated OCT B-scans at each tissue location were used by the full-spectrum probabilistic OCTA algorithm to determine the presence or absence of flow at each voxel. An investigational version of Heidelberg Eye Explorer (v. 6.16.100.701, Heidelberg Engineering, Heidelberg, Germany) was used for analysis, processing, and post-processing of data.[4] Projection artifact was removed via 3-dimensional vessel-shape estimation and a Gaussian blur filter.[4] Raw (floating point) data were exported as a .VOL file. Linear quadratic estimation (noise variance estimate of 0.05 and a gain of 0.8) was applied using a code designed in MATLAB version R2019b (Natick, Massachusetts: The MathWorks Inc.; 2019). Volume rendering and analysis of processed OCTA data utilized Imaris v9.5 (Bitplane, Andor Technology plc.) to visualize neovascular lesions at different angles of rotation.[30] The Filament Tracer tool was used to trace superficial arteries and veins after evaluation of dye circulation in FA. Video recording and still annotations were implemented to highlight specific details from structural and flow data.

The spatial distribution of vascular lesions was analyzed using a customized plugin in ImageJ (Creative computations, Birmingham, AL). Lesion distance from the fovea was calculated using OCT volume and NIR en face image using the plug-in 'Spectralis Browser OCT', available at https://sites.imagej.net/CreativeComputation/ . Location was documented using fovea-centered rings of the ETDRS grid. Location was also documented in quadrants, like the vortex drainage system.

Histology preparation and image analysis

As described, [31] globes were recovered 2:05 hours after death, fixed in 1% paraformaldehyde and post-fixed in 2.5% glutaraldehyde buffer. Pre-mortem eye-tracked OCT volumes were registered to post-mortem OCT volumes of the same globes, as described.[32] A rectangular tissue block containing fovea and optic nerve was post-fixed

in 1% osmium – tannic acid – paraphenylenediamine (OTAP) and embedded in epoxy resin. A tissue block 8 mm x12 mm wide was processed for stepped sections at 30-60 µm intervals. Interleaved 30 µm-thick slabs were re-embedded for transmission electron microscopy (TEM). Sub-micrometer sections stained with toluidine blue were scanned using a 60X oil immersion objective as described.[33] Tissue sections on 112 (right eye) and 87 (left eye) glass slides spanning a distance of 5453 µm (right eye) and 4243 µm (left eye) were matched to clinical OCT scans by comparing overall tissue contours.

DRAMA vessels are defined by a size criterion (>50 µm),[25] and our previous and current observations indicated that a collagenous sheath surrounds neovessels in type 3 MNV. Further, OCTA shows only the moving blood cell column and not the collagenous sheath. Therefore, we manually measured internal and external cross-sectional diameters of vessels in scanned images ('oval' tool, FIJI Is Just; ImageJ 2.0.0-rc-69/1.52p; www.fiji.sc;). Type 3 MNV vessels meandered over several glass slides and sections on each slide were measured on all of them. In addition, DCP vessels on either side of the area directly involved in exudation were also measured. To contextualize vessel measurements in the index case, vessels in sections through the macula of age-similar controls and intermediate AMD eyes (n= 8 each) on the Project MACULA website of AMD histopathology were also measured.[26] These were aligned along the outer border of the INL. Inner (luminal) and external vascular diameters were measured. Because vessels could run longitudinally within a section, we report a minimal cross-section diameter (approximated by Feret diameter in ImageJ for ellipses).
Due to small numbers, data were not analyzed statistically.

Results

At initial presentation 5 years before death (not shown), the right eye exhibited multiple instances of type 3 MNV secondary to AMD showing multifocal leakage on FA. On near-infrared reflectance, the left eye showed non-exudative AMD features including subretinal drusenoid deposits and soft drusen with hypo- and hyperreflective appearances, respectively, across the central macula. At this time, fluid was not detected in the left eye (not shown). Eleven months before death (**Figure 1**), and 4 years after the initial diagnosis in the right eye, the left eye was diagnosed with exudative type 3 MNV due to AMD. By this time, the patient's right eye had received 32 intravitreal anti-VEGF injections at intervals of 4-8 weeks and had experienced 4 fluid resorption cycles.

Multimodal imaging 11 months before death, when the left eye exhibited type 3 MNV, is shown in **Figure 1**. Venous and recirculation phase FA showed multiple points of hyperfluorescent leakage in both eyes (**Figure 1A & 1D**). As shown in **table 1**, lesions were numbered and assigned to zones of the ETDRS grid. [34,35] Six of 7 hyperfluorescent lesions were confirmed as vascular by histology. Vascular lesion morphology was categorized as tangled type 3 MNV (n=1), pyramidal type 3 MNV (n=2), or DRAMA when the anomalous vascular elements extended posterior to the DCP, but remained confined to the HFL (n=3).[4] One hyperfluorescent lesion could not be correlated to histology (**Supplementary figure 3A**). In addition to vascular lesions, hyperfluorescent lesions on FA due to window defects in the right eye were detected and reported elsewhere.[36]

<u>Anti-VEGF treated pyramidal (OD 2, OS 4) and tangled (OD 1) type 3 MNV</u>

On en face OCTA (**Figure 2A1**) and B-scan with flow overlay (**Figure 2A2**) in the right eye, persistent flow signal was visible within a tangled (OD 1) and a previously-reported[4] pyramidal type 3 MNV lesion (OD 2)**.** A similar pyramidal lesion (OS 4) was shown in the left eye with minimal leakage on recirculation phase FA (**Figure 3A1**), corresponding on OCT to a vertically oriented lesion with heterogeneous hyperreflectivity,

surrounded by minimal intraretinal fluid in the inner nuclear layer (INL) (**Figure 3A2**). This was the first occurrence of type 3 MNV in the left eye, and intravitreal anti-VEGF therapy was initiated. Seven months later, OCT showed increased intraretinal fluid in the INL and Henle fiber layer (HFL) surrounding the tangled (OD 1) and pyramidal (OS 4) type 3 MNV lesions as well as subsidence of the ELM in both eyes (**Figure 2B1, Figure 3B2 respectively**). The RPE/BrM complex was split by hyporeflective material producing a double layer sign, especially in the right eye (**Figure 2B1**).[37] Nine months later at the last clinical visit, OCT showed reduced intraretinal fluid, adjacent to both pyramidal and tangled type 3 MNV lesions (**Figure 2C2, Figure 3C1 respectively**). Numerous hyperreflective foci (HRF) were present in the INL of the left eye (**Figure 3C1**).

Histologic analysis revealed components of tangled (OD 1) and pyramidal (OS 4) type 3 MNV complexes (**Figure 2D, Figure 3D respectively**). Magnified views of the histology showed a tangled complex of neovessels spanning 249 µm horizontally towards the superior perifovea (**Supplementary Figure 1**). The tangled complex was partly ensheathed by collagenous material and flanked by RPE cells, two of which rested entirely within the OPL/INL. The OPL/INL border subsided where the vascular lesion extended through the HFL/ONL (**Supplementary Figure 1** panel C) and adhered to persistent BLamD draping a calcified druse (d). BrM appeared intact with no evidence of a choroidal contribution to the MNV lesions, and no evidence of MNV contributing to the OCT double layer sign. The ELM subsided at both edges of the calcified druse (yellow arrows in **Supplementary Figure 1** panel B). OD1 vessels within the INL were moderately dilated suggesting drainage venules.[38] Vessel walls of the tangled complex did not exhibit obvious arterial or venous features. Other than the vertical orientation and pyramidal morphology, the vessel complex in pyramidal type 3 MNV (OD 1) possessed the same histological features as the tangled type 3 MNV (OS 4), mentioned above (**Figure 4**).

By transmission electron microscopy, vessel walls of tangled type 3 MNV displayed endothelial cells and pericytes (**Figure 5A**). Endothelial cells in this complex did not display fenestrations (**Figure 5B**). Other vessel wall components, e.g., smooth muscle cells, connective tissue, or a 3-layer arterial configuration, could not be identified. Changes in the electron density and packing of RPE cell organelles, consistent with transdifferentiation, were observed. Atop the calcified druse, in RPE cells arrayed from the druse edge towards the druse top, lipofuscin becomes less electron-dense, and nuclei become more electron-dense (**Figure 5E**). Transmission electron microscopy for pyramidal type 3 MNV (OD 2) was not available.

Tangled type 3 MNV (OD 1) volume rendering of structural OCT and OCTA together, as displayed in **Figure 6,** highlighted neovascular blood flow within a hyperreflective tangle at the ONL (white arrowheads) and photoreceptor level (**Figure 6A**). Inflow and outflow vessels were readily connected to a superficial artery and vein, respectively (**Figure 6B&C**). A complete volume rendering of structural OCT and OCTA together are provided in **Supplementary video 1**. Lesions in the left eye were not imaged by OCTA.

<u>DRAMA, in the setting of anti-VEGF therapy</u>

All three instances of DRAMA (OS1, OS3, and OD3) were located above an intact and unaffected ELM in the inner retina. Mild hyperfluorescence on venous and recirculation phase FA is shown 11 months before death (**Figure 7A, Figure 8A, and Figure 10A, respectively**).

In histology of OS 1, a stretched vessel sagging from the INL into the ONL could be appreciated (**Figure 7A**). Similar to the type 3 MNV instances mentioned above, this lesion was located above a soft druse with BLamD and altered RPE at its apex (**Figure 7C**). Unlike type 3 MNV, on histology OS1 did not display a collagenous sheath, and the OPL did not subside.

Corresponding to FA, OCT of OS3 showed an intraretinal hyperreflective, stacked lesion, and no intraretinal cysts (**Figure 8A**). Over time, a plume of HRF extended nasally without evidence of cysts (**Figure 8C**).[39, 40] In histology, an RPE tower atop a soft druse extended into the OPL (**Figure 8D**) and a hand-shaped complex of RPE cells surrounding a vessel sagging from the DCP (**Figure 9A&B**). By light microscopy, the sagging vessel in OS3 resembled OS1 (DRAMA) in its location above a soft druse with thick BLamD and a thinned RPE layer. By transmission electron microscopy, OS3 (**Figure 9**) looked like the type 3 MNV instances described above (**Figure 5**). Vascular endothelial cells lacked evidence for fenestrations (**Figure 9C**). Other vessel wall components could not be identified. The surrounding tower of RPE was multicellular, with some multinucleated cells. Organelle packing and electron-density was similar to in-layer RPE cells (**Supplementary figure 2)**.

Another DRAMA complex (OD3) with OCTA flow overlay showed an intraretinal hyperreflective lesion containing a pair of vascular outpouching (**Figure 10C**). Corresponding histology displayed a pair of sagging vessels without significant intraretinal fluid (**Figure 10D**). Like the type 3 MNV instances described above, the vessel complex was ensheathed by collagenous material and dives from the INL into the HFL (**Figure 11A**). Moreover, RPE organelles from the edge of an underlying druse are shown at the lower edge of the vessel complex (fuchsia arrowhead, **Figure 11B**). Unlike the type 3 MNV lesions, the vessels did not extend past the HFL and there was no subsidence of the ELM, which was intact.

<u>Vessel diameters of vascular lesions and comparison vessels</u>

Supplementary table 1 shows internal and external vessel diameters of type 3 MNV and DRAMA in the index case. We compared these to nearby DCP vessels in the index case, and 8 intermediate AMD (83.4 ± 11.6 years) and 8 age-similar controls (84.1 ± 6.7 years), together called the comparison vessels.

Five of the 6 index case lesions were noticeably larger (2.5-3-fold) than the comparison vessels. External vessel diameters of type 3 MNV (OD1, OD2, OS4 15.02 µm ± 3.81 µm; 21.35 µm ± 10.79 µm; 12.46 µm ± 0.95 µm, respectively) were larger than DCP vessel diameters in the surrounding tissue (7.18 µm ± 1.11 µm). They were also larger than vessel diameters in intermediate AMD (6.79 µm ± 1.05 µm) and age similar controls (7.86 µm ± 1.47 µm, **Supplementary table 1A**). In DRAMA, external vessel diameters of OS1 and OS3 (13.39 µm ± 2.68 µm; 17.97 µm ± 1.08 µm) were considerably larger than the comparison vessels. A similar pattern was seen for internal vessel diameters (**Supplementary table 1B**).

Discussion

In two anti-VEGF treated eyes with multifocal intraretinal neovascular AMD, we directly compared longitudinal clinical multimodal imaging and histology. New insights in type 3 MNV and DRAMA are provided through analysis of six histologically confirmed vascular lesions. Different vascular phenotypes, specific spatial distribution across and within the retina, and specific vessel features were identified.

Treated type 3 MNV has two morphologic phenotypes, as seen in 3 of 7 histologically confirmed lesions (OD1, OD2, OS4). On histology, these lesions showed a pyramidal (OD2, OS4) or tangled (OS4) phenotype. All three complexes originated at the DCP and extended posteriorly through the RPE to infiltrate BLamD but were not found to penetrate BrM. We believe these types correspond to those described by Sacconi et al in 15 treatment-naïve type 3 MNV eyes investigated with rotational three-dimensional OCTA. These authors described 26 lesions as ‘filiform’ and 9 lesions as ‘saccular’, which appear similar in shape to pyramidal (filiform) and tangled (saccular).[15] Similarly, in our patient, we found the pyramidal phenotype to be more prevalent than the tangled morphology. As location and point of onset of saccular and filiform phenotypes were not reported,[15] and we observed both phenotypes in our case at initial presentation, it remains to be determined if saccular and filiform lesions differ in spatial distribution and time of onset.

All three type 3 MNV lesions were localized within 500-1520 µm of the foveal center, in line with recent reports of similar findings for solitary and multifocal type 3 MNV. [12, 13] It has been hypothesized that type 3 MNV is associated with choroidal ischemia,[12, 41-43] because the choroid is significantly thinner in type 3 MNV than age-matched controls with types 1 and 2 MNV.[44, 45] The radial symmetry around the fovea further suggests an association with the distribution of photoreceptors and their

supporting cells. The area of type 3 MNV vulnerability in the ETDRS inner ring is just peripheral to the foveal avascular zone[46] on the inner slope of the crest of high rod density, where rod vision is poor in AMD eyes. [47-51] Metabolic demand of foveal cones is very high, and choriocapillaris OCTA signal decreases under the fovea throughout adulthood.[52, 53] It is thus possible that the distribution of type 3 MNV is a bystander effect from changes under the fovea that also lead to high-risk drusen.

Type 3 MNV complexes show vascular features in histology similar to our previous descriptions.[17] By electron microscopy, a pyramidal type 3 MNV lesion had endothelial cells and pericytes, surrounded by a thick collagenous matrix. The thickness of this matrix distinguished lesions from unaffected DCP vessels. Unlike choriocapillaris,[54] intraretinal vessels form the inner blood-retinal barrier and do not have fenestrated endothelium.[55] In pyramidal type 3 MNV, endothelial cells accordingly lacked fenestrations, presumably reflecting the vessels of origin and possibly contributing to greater responsiveness to intravitreal anti-VEGF treatment of early type 3 MNV (retinal tissue penetration of anti-VEGF) compared to type 1 and 2 MNV.[56, 57] The main difference between pyramidal and tangled lesions was the larger horizontal component of tangled vessels, which extended along exposed BLamD draping a calcified drusein lesion. The tangled morphology seemed to resemble a previously published type 3 MNV case.[58]

Ectopic RPE cells clustered around neovessels. This is in line with the updated OCT classification system[3] and previous clinicopathologic evidence of isolated and dysmorphic RPE cells distributed along a stalk of neovascularization.[17] These data support the early involvement of migratory RPE in type 3 MNV.[3, 59] Previously reported lipid-filled non-RPE cells were not found in this case, possibly due to the prior anti-VEGF treatment or to the use of stepped sections.[17]

All type 3 MNV lesions responded to anti-VEGF with temporary resolution of exudation but persisted during the treatment period over several fluid absorption cycles. This finding may support a body of previous OCTA literature wherein some early-stage type 3 MNV lesions appear to show complete regression following initiation of anti-VEGF therapy while treatment of later stage type 3 MNV may require continuous therapy.[3, 60] Given the thick collagenous sheaths of neovessel complexes on histology, it seems unlikely that the lesions could have completely disappeared due to anti-VEGF treatment in clinical imaging. However, clinical reappearance in recurrent type 3 MNV is possible after lesions became undetectable on OCTA in response to intravitreal anti-VEGF therapy.[61] Nevertheless, the persistence of this MNV subtype after treatment, may be due to thick vessel walls. If so, then type 3 MNV might require monitoring for disease activity by vascular characteristics in addition to fluid. For example, non-exudative lesions on OCT could be distinguished from lesions with and without decorrelation signal on OCTA. Lesions with decorrelation signal on OCTA, representing continuous perfusion, would then be considered for treatment or monitoring.

This case demonstrated that type 3 MNV can coexist with other vascular formations that are candidates for precursors, early stages, and masqueraders. Four intraretinal vascular lesions in our sample were considered DRAMA. All four originated from the DCP and extended posteriorly into the HFL but did not reach the ONL. The DRAMA were located within the inner ring of ETDRS and were ensheathed in collagen, possibly indicating a role as a precursor of type 3 MNV. Like the pyramidal type 3MNV, ultrastructural vessel wall features in one DRAMA (**figure 9**) showed endothelial cells and pericytes with a thin collagenous sheath, without fenestrations. Importantly, none of the DRAMA were accompanied by descent of the ELM, the border of atrophy in neurosensory retina, although the ELM could be perforated as in OS3. It is unlikely that these vessels are exudative or non-exudative perifoveal vascular anomalous complexes

(ePVAC/ nePEVAC).[31,35,36] Our lesions were located below the DCP, not between the SCP and DCP, typically for ePVAC and nePEVAC. In a recent study of 25 eyes with type 3 MNV most cases exhibited on OCT an asymptomatic precursor stage.[62] Non-neovascular microvascular anomalies associated with locally increased VEGF expression[63, 64] include capillary dilations and telangiectasia in eyes with neovascular AMD and non-neovascular AMD.[18, 63, 65] None of our 4 DRAMA lesions involved the SCP on OCTA and histology, and no significant intraretinal fluid was detectable on OCT over time. It is possible that lack of exudation and non-progression to ~~typical~~ type 3 MNV might be a result of the treatment.[66] Longitudinal imaging is required to definitively place DRAMA in the progression sequence of type 3 MNV and determine treatment approaches.

Study strengths include the availability of OCTA imaging with eye-tracked OCT, rapid preservation of the globes that largely maintained retinal attachment, and comprehensive histologic, photomicroscopy, and ultrastructural techniques to reveal vessels and perivascular tissue elements. In addition, registration of pre-mortem eye-tracked OCT volumes to post-mortem OCT volumes of the same globes allows for true in vivo-ex vivo correlation of retinal biomarkers.[33] Limitations include the lack of longitudinal OCTA imaging to visualize anti-VEGF treated vessels over time, [10, 67] and lack of color fundus photography to reveal discoloration patterns typical of type 3 MNV.[14] Limitations to the laboratory study included use of stepped sections that may have missed details such as retinal vascular connections with the choriocapillaris, lack of electron microscopy for all lesions, and lack of immunohistochemistry to support cell type identifications based on published morphologic criteria alone. Finally, this report presents a clinicopathologic correlation of two eyes of one patient and cannot elucidate the full range of biologic variability.

Despite these limitations, our data helped define morphologies of type 3 MNV and offered candidate precursors than might guide diagnosis and disease monitoring in the future. Further investigation with longitudinal imaging before exudation onset is needed to distinguish among these entities. Improved resolution in current imaging modalities, introduction of new techniques, and multimodal imaging including OCTA will provide new insights and better understanding in disease mechanisms and identification of new entities.[5] Our histologically validated OCT and OCTA signatures of vascular lesions in anti-VEGF treated type 3 MNV can serve as a valuable reference for such studies.

Acknowledgments

Contribution statement

All authors were involved in drafting the article or revising it critically for important intellectual content, and all authors approved the final version to be published. Dr. Curcio and Dr. Berlin had full access to all the data in the clinical picture and take responsibility for the integrity of the data and the accuracy of the data analysis. Study conception and design: AB, DC, LC, CB, RM, DF, KBF, CC. Acquisition of data: RM, CB, JM, LC, AB, DC, KBF, CC. Analysis and interpretation of data: AB, DC, LC, DF, KBF, CC. Writing of manuscript: AB, DC, CB, LC, RM, DF, KBF, CC.

Financial support

This work was supported by Genentech/ Hoffman LaRoche, The Macula Foundation, Inc., New York, NY; unrestricted funds to the Department of Ophthalmology and Visual Sciences (UAB) from Research to Prevent Blindness, Inc., and EyeSight Foundation of Alabama. AB reports grants from the Dr. Werner Jackstädt-foundation. DC was supported in part by a studentship from Fundação Luso-Americana para o desenvolvimento (FLAD, USA R&D@PhD – Proj 2020/0140). Purchase of the slide scanner was made possible by the Carl G. and Pauline Buck Trust.

The sponsors had no role in the design and conduct of the study; collection, management, analysis, and interpretation of the data; preparation, review, or approval of the manuscript; and decision to submit the manuscript for publication.

Financial disclosure

KBF is a consultant to Genentech, Zeiss, Heidelberg Engineering, Allergan, Bayer, and Novartis. CAC receives research funds from Regeneron (outside this project). DF is an employee of Genentech and a stockholder of Roche.

Meeting presentation

This work was submitted as part of an abstract to the annual meeting of The Association for Research in Vision & Ophthalmology (ARVO) May 2021 and May 2022.

Figures

High resolution figures and supplementary figures can be downloaded here:

https://uab.box.com/s/46p3zi9zafcsepv1stcx8ijow3g9mjy2

Figure 1. Multimodal retinal imaging of both eyes, 11 months before death.
FA, fluorescein angiography; FAF, fundus autofluorescence (488 nm); NIR, near-infrared reflectance (scale bar 200 µm); arrowheads (yellow, fuchsia, and green), confirmed vascular lesions by histology corresponding to hyperfluorescence on FA; white arrowhead, hyperfluorescent lesion without corresponding vascular lesion by histology. Lesion number, type, and spatial distribution are listed in **table 1**.
A & **D**. Venous (**A**) and recirculation phase (**D**) FA showing hyperfluorescence at the green, yellow, and fuchsia arrowheads in the right (**A**), and left eye (**D**) were identified by histology. Vascular correlate for hyperfluorescence at the white arrowhead in the left eye was not found in histology.
B & **E**. NIR, areas at arrowheads show reduced reflectance in areas of angiographic leakage, possibly due to retinal edema.
C & **F**. FAF, subretinal drusenoid deposits especially in the superior hemisphere and soft drusen with hypo- and hyperreflective mottling in the central macula.

Figure 2. Multimodal imaging and clinical course of tangled type 3 MNV, OD1.
Green arrowhead, type 3 MNV; green lines, optical coherence tomography (OCT) B-scans; red lines, portions of B-scan shown in panels A2, B1, and C1; blue line in **C**, histology section; Time in months, time before death; FA, fluorescein angiography; BCVA, best acuity visual acuity.
A. Near-infrared reflectance (NIR, **A**), en face OCT angiography (OCTA, **A1**), and OCT B-scan with flow signal overlay (**A2**). There is persistent flow signal within the tangled hyperreflective type 3 MNV lesion, after 29 total injections and 8 weeks following the prior injection. The RPE/Bruch's membrane complex is split by hyporeflective material and appears as a "double layer" sign without flow signal. Red lines in **A2** indicate the segmentation boundaries [outer plexiform layer (OPL)-retinal pigment epithelium (RPE)] used to create the en face OCTA (**A1**). **B**. FA (**B**) shows late venous phase hyperfluorescence. OCT B-scan (**B1**) shows intraretinal fluid in the inner nuclear and Henle fiber layers surrounding the type 3 MNV lesion, after 32 total injections and 8 weeks following the last injection. **C**. NIR (**C**) and radially oriented OCT B-scan (**C1**),

after 36 total injections and 8 weeks following the last injection. The OCT B-scan shows intraretinal fluid adjacent to the tangled type 3 MNV lesion. **D**. Histology shows a horizontally oriented tangled type 3 MNV lesion, partly bounded by RPE cells (scale bar 200 µm). The complex extends from the inner nuclear layer border to basal laminar deposit that drapes a calcified druse plateau lacking RPE at its apex. The double layer sign in B1 is not corresponding to neovascularization.

Figure 3. Multimodal imaging, clinical course, and histology of pyramidal type 3 MNV, OS4.

Green arrowhead, hyperreflective lesion; green lines, optical coherence tomography (OCT) B-scans; blue line, histology section. Time in months, time before death; FA, fluorescein angiography.

A. **A1,** Venous phase FA shows mild leakage at site of type 3 MNV; **A2,** small intraretinal cysts and hyperreflective foci (HRF) are evident.

B. **B2,** after 4 injections (8-week interval), intraretinal cysts enlarged, and the outer plexiform layer (OPL) and external limiting membrane subsided.

C.**C2**, after 6 injections (6-week interval), intraretinal fluid is reduced. Numerous HRF are present in the inner nuclear layer (INL, scale bar 200 µm).

D. On histology, type 3 MNV is a pyramidal complex bounded by RPE cells (scale bar 100 µm). It extends from the OPL/INL border to basal laminar deposit that drapes a calcified druse. Structural damage to Henle's fiber layer at the right of the panel may indicate an area of prior intraretinal fluid (green asterisk). Magnified histology in **figure 4**.

Figure 4. Pyramidal vascular complex in type 3 MNV, OS4.

A, B. A pyramidal complex includes neovessels ensheathed by collagenous material and flanked by RPE cells, some of which rest entirely within the Henle fiber layer (HFL). The complex extends from the outer plexiform layer (OPL)/ inner nuclear layer through the HFL/outer nuclear layer and infiltrates Basal laminar deposits draping a calcified druse. Bruch's membrane appears intact with no evidence of a choroidal contribution to the MNV lesion. The external limiting membrane descends on both sides of the lesion base. There is some fluid at the OPL-HFL border (yellow asterisk in **B**). Transmission electron microscopy of the areas within dotted green boxes are shown in **Figure 5**.

Figure 5. Transmission electron microscopy of pyramidal type 3 MNV, OS4.

A. Neovessel ensheathed by pericyte, endothelial cell, and collagenous material (white, purple, and black asterisks, respectively).

Erythrocyte fills the lumen (blue asterisk). Surrounding retinal pigment epithelium (RPE) cells merge into multi-nucleated cells or disperse into the outer nuclear layer/Henle's fiber layer (red, green asterisks, respectively). Phagolysosomes are not visible in RPE.

B-D. Endothelial cell ultrastructure in neovessel and comparison vessels. Lumen is at the bottom of all panels.

B. No fenestrations are detected in the neovessel (orange arrowheads).

C. Fenestrations are visible in the choriocapillaris (orange arrowheads).

D. No fenestrations are detected in the deep capillary plexus (orange arrowheads).

E. Atop the calcified druse (fuchsia asterisk), in RPE cells arrayed from the druse edge towards the druse top (left to right in the panel), lipofuscin becomes less electron-dense, and nuclei (green and yellow arrowheads) become more electron-dense. These changes are consistent with transdifferentiation.

Figure 6. Volume rendering showing structural OCT (gray) and OCTA (yellow) of tangled type 3 MNV, OD1.

A. Neovascular blood flow within a hyperreflective structure is observed at the outer nuclear layer (white arrowheads) and photoreceptor level.

B. Three-dimensional analysis of neovascular blood flow depicted an anastomosis right above the RPE/Bruch's membrane (green section) and a tangled structure connecting to the superficial artery (red arrow) and vein (blue arrow).

C. Volume rendering of OCTA with orthogonal structural sections centered on the lesion evidenced a tangled neovascular lesion.

Figure 7. Deep retinal age-related microvascular anomaly (DRAMA), OS 1.

yellow arrowheads, hyperreflective sagging vessel; green lines, optical coherence tomography (OCT) B-scans; blue line, histology section; FA, fluorescein angiography; NIR, Near-infrared reflectance, subretinal drusenoid deposits, SDD.

A. Baseline NIR shows drusen and SDD. B. Recirculation phase FA shows minimal leakage at the site of DRAMA.

C. In histology, a stretched vessel sags from the inner nuclear layer into the outer plexiform layer above a soft druse with basal laminar deposit and altered retinal pigment epithelium at its apex.

Figure 8. In vivo OCT: Deep retinal age-related microvascular anomaly (DRAMA) or precursor of type 3 MNV, OS3.

Fuchsia arrowhead, hyperreflective lesion; green lines, optical coherence tomography (OCT) B-scans; blue line, histology section; time in months, time before death; FA, fluorescein angiography; HRF, hyperreflective foci.

A. Baseline images show faint venous phase FA staining, intraretinal hyperreflective stacked lesion, and no intraretinal cysts.

B, C. After 4 (**B**) and 6 (**C**) injections (8 and 6-week intervals), the lesion is stable, without cysts. A plume of HRF extends nasally.

D. In histology, a retinal pigment epithelium tower based on a soft druse surrounds a vessel and extends into the outer plexiform layer. Magnified histology is shown in **figure 9**.

Figure 9. Deep retinal age-related microvascular anomaly (DRAMA) or precursor of type 3 MNV, OS3.

A. A “hand” shaped complex consisting of RPE cells surrounds a sagging vessel from the deep capillary plexus. Electron microscopy of the area in the fuchsia box is shown in Supplementary Figure 2.

B. RPE complex extends through the Henle fiber layer/outer nuclear layer (ONL) into the outer plexiform layer (OPL) and inner nuclear layer, possibly reaching the intermediate capillary plexus. There is no subsidence of OPL or external limiting membrane. The ONL is thinned. The complex rests on a base of basal laminar deposit (BLamD) and a soft druse that is detached from Bruch’s membrane.

C-E. Endothelial cell ultrastructure in DRAMA and comparison vessels. Lumen with blood cells is at the bottom of all panels. Endothelial cell, EC.

C. No fenestrations are visible in the DRAMA (red blood cell, RBC).

D. No fenestrations are visible in the deep capillary plexus (pericyte, P). The lumen is off the bottom of this panel.

E. Fenestrations are visible in the choriocapillaris endothelium (orange arrowheads; white blood cell, WBC).

Figure 10. Multimodal imaging of type 3 MNV precursor or deep retinal age-related microvascular anomalies (DRAMAs), OD3.

Fuchsia arrowheads, DRAMA complex; green lines, optical coherence tomography (OCT) B-scans; blue line, histology section.

FA, venous phase mild hyperfluorescence 11 months before death. **B**. NIR; **C**. Horizontally oriented OCT scan with OCTA flow overlay (**C**) shows cyst like spaces in the Henle fiber layers adjacent to the tangled hyperreflective lesion. The retinal pigment epithelium/Bruch's membrane complex to the left is split by hyporeflective material. **D**. The OCTA flow signal shows a pair of intraretinal flow corresponding to a pair of outpouchings, deep retinal age-related microvascular anomalies. **E.** Histology shows a thickened choroid to the left (temporal) to a pair of sagging vessels, retinal age-related microvascular anomalies. The complex extends from the inner nuclear layer border to the outer nuclear layer. Magnified histology is shown in **figure 1**.

Figure 11. Vascular complex of type 3 MNV precursor or deep retinal age-related microvascular anomalies (DRAMAs) in type 3 MNV, OD3.

A, B. A "sagging" pair of vessels, (DRAMA complex, fuchsia arrowheads) ensheathed by collagenous material dives from the INL into the Henle's fiber layer (HFL)/outer nuclear layer (ONL). Next to it is a degenerative cyst in the HFL. There is no subsidence of external limiting membrane. The ONL is thinned.

C. RPE from the edge of a druse migrates towards the lower edge of the vessel complex.

Table 1. Spatial distribution and vascular lesion types in treated type 3 MNV eyes.

Eye, lesion number, color in Fig. 1	Distance to fovea (µm)	ETDRS quadrants	Vortex vein quadrants	Lesion type	intravitreal anti-VEGF
OD1 (green)	520*	S	ST	T3MNV, tangled	37
OD2 (yellow)	1154	N	SN	T3MNV, pyramidal	37
OD3 (fuchsia)♦	602	T	IT	DRAMAs	37
OS1 (yellow)	1305	S	ST	DRAMA	6
OS2 (white)	1520	I	IT	not found	6
OS3 (fuchsia)	1164	I	IT	DRAMA	6
OS4 (green)	1101	N	ST	T3MNV, pyramidal	6

Table 1. Spatial distribution of and lesion type in treated type 3 MNV.

T3MNV, type 3 macular neovascularization; DRAMA, deep retinal age-related microvascular anomaly; n.a., not applicable; ETDRS quadrants: S, superior; I, inferior; N. nasal; T, temporal; Vortex vein quadrants: ST, superior temporal; SN, superior nasal; IN, inferior nasal; IT, inferior temporal.

Within each eye. lesions were numbered clockwise, starting at 12:00 in the ETDRS grid. Spatial distribution was documented according to quadrants in the ETDRS grid and vortex vein drainage systems. The ETDRS grid system is divided by 45° lines, resulting in 4 spatial descriptors (nasal, temporal, superior, and inferior). The vortex vein system is divided by 90° lines due to the area of blood drainage, resulting in 4 different descriptors (superior-temporal, superior-nasal, inferior-temporal, and inferior-nasal). In total 7 lesions could be identified on fluorescein angiography. Six lesions were located within 500 to 1500 µm of the fovea, corresponding to the inner ring of the ETDRS grid. One lesion was located outside the 1500 µm ring (1520 µm), corresponding to the outer ring of the ETDRS grid. In addition to vascular lesions, hyperfluorescence on fluorescein angiography due to window defects was detected, as reported elsewhere *(cite RCBR report)*. * Span width of tangled vascular lesion: 520-769 µm; ♦ pair of vascular lesions.

Supplementary Figures, Video, and Tables

Supplementary Figure 1. Tangled vascular complex in type 3 MNV, OD1.

Fuchsia arrowheads, lumen of type 3 MNV complex; Light blue arrowhead migrated RPE; yellow arrowhead, ELM descend; Fuchsia asterisks, BLamD.

A-C. Tangled vascular complex spanning 249 µm horizontally towards the superior perifovea. The complex is partly ensheathed by collagenous material and is flanked by RPE cells, two of which rest entirely within the OPL/INL (light blue arrowhead in **A,** 759 µm from fovea, fuchsia arrowhead on the right in **B,** 719 µm from fovea) The OPL/INL, subsides (**C,** 552 µm from fovea) and the vascular complex extends from the OPL/INL border through the HFL/ONL. The complex adheres to BLamD draping a calcified druse plateau (d). Bruch's membrane appears intact with no evidence of a choroidal contribution to the MNV lesions. The ELM descends at both edges of the calcified druse plateau (yellow arrowheads in **B**). Vessel walls do not exhibit obvious arterial or venous features. Vessel diameter within the INL was larger than 15 µm, suggesting drainage venules.

Supplementary Figure 2.

Transmission electron microscopy of DRAMA, OS3.

Vessel is ensheathed by endothelial (E) cells and pericytes (P), with little collagen. Lumen contains leukocytes (LC) and erythrocytes (RBC). Surrounding tower of RPE is multicellular (white asterisks), and multinucleated (fuchsia asterisks). Retinal pigment epithelium (RPE) organelle packing and electron-density is similar to in-layer RPE cells (not shown).

Supplementary Figure 3. Hyperfluorescence without histologic correlate, OS2.

White arrowhead, hyperreflective lesion; green lines, optical coherence tomography (OCT) B-scans; blue line, histology section. Time in months, time before death; FA, fluorescein angiography.

A. Venous phase FA hyperfluorescence, drusen, double-layer sign with hyper-transmission and hyperreflective foci (HRF).

B, C. After 4 (B) and 6 (C) injections, the lesion is stable, without cysts.

Supplementary video 1.

Volume rendering of structural OCT (gray) and OCTA (yellow) of tangled type 3 MNV, OD1 (Fig. 6).

The cube was rotated 180° to highlight vascular findings in the superior macula region. Coronal view demonstrates blood flow immediately below the deep capillary plexus level in two separate areas. Superposition with structural OCT (gray channel) demonstrates neovascular blood flow within an hyperreflective structure at the outer nuclear layer and above Bruch's membrane. The superficial arteries (red) and veins (blue) in the vicinity of the lesion were outlined after fluorescein angiography analysis. Three-dimensional analysis of neovascular blood flow depicted an anastomosis right above BrM (green section) Spinning around the neovascular blood-flow highlights separate inflow and outflow.

Supplementary Table 1. Diameters of vessels in histology

A. External vessel diameter (µm)

	T3 MNV*			DRAMA*			T3 DCP†	Control†	AMD†
	OD1	OD2	OS4	OS1	OS3	OD3			
Mean	15.02	21.35	12.46	13.39	17.97	8.62	7.18	7.86	6.79
SD	3.81	10.79	0.95	2.68	1.08	1.05	1.11	1.47	1.05

B. Internal vessel diameter (µm)

	T3 MNV*			DRAMA*			T3 DCP†	Control†	AMD††
	OD1	OD2	OS4	OS1	OS3	OD3			
Mean	9.34	14.86	9.87	9.40	8.28	5.17	3.69	4.44	3.75
SD	1.85	6.19	0.76	2.00	0.31	0.34	0.92	0.98	0.92

* 3 to 6 measurements for each; T3 MNV, type 3 macular neovascularization; DRAMA, deep retinal age-related microvascular anomaly.
† 8 female control eyes (84.1 ± 6.7 years; 1 male and 7 female), intermediate AMD eyes (83.4 ± 11.6 years). Histology from Project MACULA https://projectmacula.org.
Number of measurements, Type 3 DCP (n=123); Controls (n=88); AMD (n=107).
OS2 no lesion identified in histology.

References

1. Freund KB, Zweifel SA, Engelbert M. Do we need a new classification for choroidal neovascularization in age-related macular degeneration? Retina. 2010 Oct;30(9):1333-49.
2. Spaide RF, Noble K, Morgan A, Freund KB. Vitelliform macular dystrophy. Ophthalmology 2006;113(8):1392-400. e4.
3. Su D, Lin S, Phasukkijwatana N, et al. An Updated staging system of type 3 neovascularization using spectral domain optical coherence tomography. Retina 2016;36:S40-S9.
4. Berlin A, Cabral D, Chen L, et al. Correlation of optical coherence tomography angiography of type 3 macular neovascularization with corresponding histology. JAMA Ophthalmology 2022.
5. Spaide RF, Jaffe GJ, Sarraf D, et al. Consensus nomenclature for reporting neovascular age-related macular degeneration data: consensus on neovascular age-related macular degeneration nomenclature study group. Ophthalmology 2020;127(5):616-36.
6. Yannuzzi LA, Negrão S, Tomohiro I, et al. Retinal angiomatous proliferation in age–related macular degeneration. Retina 2012;32:416-34.
7. Chen KC, Jung JJ, Curcio CA, et al. Intraretinal hyperreflective foci in acquired vitelliform lesions of the macula: clinical and histologic study. American journal of ophthalmology 2016;164:89-98.
8. Kim JH, Kim JW, Kim CG, Lee DW. Influence of fellow-eye examination interval on visual acuity at fellow-eye neovascularization in unilateral type 3 neovascularization. Retina 2020;40(7):1255-61.
9. Kwak JH, Park WK, Kim RY, et al. Unaffected fellow eye neovascularization in patients with type 3 neovascularization: incidence and risk factors. PloS One 2021;16(7):e0254186.
10. Sacconi R, Forte P, Capuano V, et al. OCT-A characterization of evolving lesions in fellow eyes of exudative type 3 MNV patients. Retina 2022:10.1097.
11. Freund KB, Ho I-V, Barbazetto IA, et al. Type 3 neovascularization: The expanded spectrum of retinal angiomatous proliferation. Retina 2008;28(2):201-11.
12. Najeeb BH, Deak G, Schmidt-Erfurth U, Gerendas BS. The Rap Study, Report Two: the regional distribution of macular neovascularization type 3, a novel insight into its etiology. Retina 2020;40(12):2255-62.
13. Haj Najeeb B, Deak GG, Sacu S, et al. The Rap Study, Report 4: morphological and topographical characteristics of multifocal macular neovascularization type 3. Graefe's Archive for Clinical and Experimental Ophthalmology 2022;260(1):141-7.
14. Haj Najeeb B, Deak GG, Schmidt-Erfurth U, Gerendas BS. The Rap Study, Report 3: discoloration of the macular region in patients with macular neovascularization type 3. Acta Ophthalmologica 2021.
15. Borrelli E, Sacconi R, Klose G, et al. Rotational Three-Dimensional OCTA: a notable new imaging tool to characterize type 3 Macular neovascularization. Scientific Reports 2019;9(1):1-8.
16. Shimada H, Kawamura A, Mori R, Yuzawa M. Clinicopathological findings of retinal angiomatous proliferation. Graefe's Archive for Clinical and Experimental Ophthalmology 2007;245(2):295-300.
17. Li M, Dolz-Marco R, Messinger JD, et al. Clinicopathologic correlation of anti–vascular endothelial growth factor–treated type 3 neovascularization in age-related macular degeneration. Ophthalmology 2018;125(2):276-87.
18. Sacconi R, Freund KB, Yannuzzi LA, et al. The expanded spectrum of perifoveal exudative vascular anomalous complex. American Journal of Ophthalmology 2017;184:137-46.
19. Gilani F, Gal-Or O, Freund KB. Spontaneous rupture and involution of a “macro–microaneurysm” in diabetic retinopathy. Retina 2017;37(6):e73-e4.

20. Spaide RF, Barquet LA. Retinal capillary macroaneurysms. Retina 2019;39(10):1889-95.
21. Sacconi R, Cohen SY, Borrelli E, et al. Correspondence. Retina 2019;39(11):e48-e9.
22. Spaide RF. Correspondence Reply. Retina 2019;39(11):E49-E50.
23. Sacconi R, Borrelli E, Sadda S, et al. Nonexudative perifoveal vascular anomalous complex: The subclinical stage of perifoveal exudative vascular anomalous complex? American Journal of Ophthalmology 2020;218:59-67.
24. Querques G, Kuhn D, Massamba N, et al. Perifoveal exudative vascular anomalous complex. Journal Français d'Ophtalmologie 2011;34(8):559. e1-. e4.
25. Cabral D, Ramtohul P, Fradinho A, Freund KB. Volume rendering of deep retinal age-related microvascular anomalies. Ophthalmol Retina 2022.
26. Chen L, Messinger JD, Sloan KR, et al. Nonexudative macular neovascularization supporting outer retina in age-related macular degeneration: A clinicopathologic correlation. Ophthalmology 2020;127(7):931-47.
27. Querques G, Querques L, Forte R, et al. Precursors of type 3 neovascularization: a multimodal imaging analysis. Retina 2013;33(6):1241-8.
28. Association WM. World Medical Association Declaration of Helsinki: ethical principles for medical research involving human subjects. JAMA 2013;310(20):2191-4.
29. Edemekong P, Annamaraju P, Haydel M. Health Insurance Portability and Accountability Act. 2022 Feb 3. In: StatPearls [Internet]. Treasure Island (FL): StatPearls Publishing; 2022 Jan.
30. Xu X, Yannuzzi NA, Fernández-Avellaneda P, et al. Differentiating veins from arteries on optical coherence tomography angiography by identifying deep capillary plexus vortices. American Journal of Ophthalmology 2019; 207:363-72.
31. Balaratnasingam C, An D, Sakurada Y, et al. Comparisons between histology and optical coherence tomography angiography of the periarterial capillary-free zone. American Journal of Ophthalmology 2018;189:55-64.
32. Litts KM, Messinger JD, Dellatorre K, et al. Clinicopathological correlation of outer retinal tubulation in age-related macular degeneration. JAMA Ophthalmology 2015;133(5):609-12.
33. Balaratnasingam C, An D, Freund KB, et al. Correlation between histologic and OCT angiography analysis of macular circulation. Ophthalmology 2019;126(11):1588-9.
34. Group ETDRSR. Grading diabetic retinopathy from stereoscopic color fundus photographs—an extension of the modified Airlie House classification: ETDRS Report Number 10. Ophthalmology 1991;98(5):786-806.
35. Pongsachareonnont P, Somkijrungroj T, Assavapongpaiboon B, et al. Foveal and parafoveal choroidal thickness pattern measuring by swept source optical coherence tomography. Eye 2019;33(9):1443-51.
36. Berlin A MJ, Ferrara D, Freund KB, Curcio CA. OCT Features relevant to neovascular AMD management and non-neovascular AMD progression: clinicopathologic correlation. Retinal Cases and Brief Reports 2022,ms acceppted.
37. Berlin A, Chen L, Messinger J, et al. Double-layer sign in neovascular age-related macular degeneration–Do we treat? Acta Ophthalmologica 2022;100(3):348-9.
38. Snodderly DM, Weinhaus RS, Choi J. Neural-vascular relationships in central retina of macaque monkeys (macaca fascicularis). Journal of Neuroscience 1992;12(4):1169-93.
39. Balaratnasingam C, Messinger JD, Sloan KR, et al. Histologic and optical coherence tomographic correlates in drusenoid pigment epithelium detachment in age-related macular degeneration. Ophthalmology 2017;124(5):644-56.
40. Cao D, Leong B, Messinger JD, et al. Hyperreflective foci, optical coherence tomography progression indicators in age-related macular degeneration, include transdifferentiated retinal pigment epithelium. Investigative Ophthalmology & Visual Science 2021;62(10):34-.
41. Hayreh SS. Segmental Nature of the choroidal vasculature. British Journal of Ophthalmology 1975;59(11):631-48.

42. Hayreh SS. In vivo choroidal circulation and its watershed zones. Eye 1990;4(2):273-89.
43. Hayreh SS. Posterior ciliary artery circulation in health and disease the Weisenfeld Lecture. Investigative Ophthalmology & Visual Science 2004;45(3):749-57.
44. Yamazaki T, Koizumi H, Yamagishi T, Kinoshita S. Subfoveal choroidal thickness in retinal angiomatous proliferation. Retina 2014;34(7):1316-22.
45. Kim JH, Kim JR, Kang SW, et al. Thinner choroid and greater drusen extent in retinal angiomatous proliferation than in typical exudative age-related macular degeneration. American Journal of Ophthalmology 2013;155(4):743-9. e2.
46. Kim JH, Chang YS, Kim JW, et al. Characteristics of type 3 neovascularization lesions: focus on the incidence of multifocal lesions and the distribution of lesion location. Retina 2020;40(6):1124-31.
47. Tan R, Guymer RH, Luu CD. Subretinal drusenoid deposits and the loss of rod function in intermediate age-related macular degeneration. Investigative Ophthalmology & Visual Science 2018;59(10):4154-61.
48. Tan RS, Guymer RH, Aung K-Z, et al. Longitudinal assessment of rod function in intermediate age-related macular degeneration with and without reticular pseudodrusen. Investigative Ophthalmology & Visual Science 2019;60(5):1511-8.
49. Chen KG, Alvarez JA, Yazdanie M, et al. Longitudinal study of dark adaptation as a functional outcome measure for age-related macular degeneration. Ophthalmology 2019;126(6):856-65.
50. Zhang Y, Sadda SR, Sarraf D, et al. Spatial dissociation of subretinal drusenoid deposits and impaired scotopic and mesopic sensitivity in AMD. Investigative Ophthalmology & Visual Science 2022;63(2):32-.
51. Nigalye AK, Hess K, Pundlik SJ, et al. Dark adaptation and its role in age-related macular degeneration. Journal of Clinical Medicine 2022;11(5):1358.
52. Zheng F, Zhang Q, Shi Y, et al. Age-dependent changes in the macular choriocapillaris of normal eyes imaged with swept-source optical coherence tomography angiography. American Journal of Ophthalmology 2019;200:110-22.
53. Ingram NT, Fain GL, Sampath AP. Elevated energy requirement of cone photoreceptors. Proceedings of the National Academy of Sciences 2020;117(32):19599-603.
54. Grossniklaus HE, Green WR. Choroidal neovascularization. American Journal of Ophthalmology 2004;137(3):496-503.
55. Cunha-Vaz J. The Blood-ocular barriers. Survey of Ophthalmology 1979;23(5):279-96.
56. Hutton-Smith LA, Gaffney EA, Byrne HM, et al. Ocular pharmacokinetics of therapeutic antibodies given by intravitreal injection: estimation of retinal permeabilities using a 3-compartment semi-mechanistic model. Molecular Pharmaceutics 2017;14(8):2690-6.
57. Hutton-Smith LA, Gaffney EA, Byrne HM, et al. Theoretical insights into the retinal dynamics of vascular endothelial growth factor in patients treated with ranibizumab, based on an ocular pharmacokinetic/pharmacodynamic model. Molecular Pharmaceutics 2018;15(7):2770-84.
58. Monson DM, Smith JR, Klein ML, Wilson DJ. Clinicopathologic correlation of retinal angiomatous proliferation. Archives of Ophthalmology 2008;126(12):1664-8.
59. Spaide RF. Fundus autofluorescence and age-related macular degeneration. Ophthalmology 2003;110(2):392-9.
60. Kim JH, Chang YS, Kim JW, et al. Difference in rreatment outcomes according to optical coherence tomography–based stages in type 3 neovascularization (retinal angiomatous proliferation). Retina 2018;38(12):2356-62.
61. Sacconi R, Battista M, Borrelli E, et al. OCTA characterisation of recurrent type 3 macular neovascularisation. British Journal of Ophthalmology 2021;105(2):222-6.
62. Najeeb BH, Deak GG, Mylonas G, et al. The Rap Study, Report 5: rediscovering macular neovascularization Type 3: multimodal imaging of fellow eyes over 24 months. Retina 2022;42(3):485.

63. Tolentino MJ, Miller JW, Gragoudas ES, et al. Intravitreous injections of vascular endothelial growth factor produce retinal ischemia and microangiopathy in an adult primate. Ophthalmology 1996;103(11):1820-8.
64. Tolentino MJ, Mcleod DS, Taomoto M, et al. Pathologic features of vascular endothelial growth factor-induced retinopathy in the nonhuman primate. American Journal of Ophthalmology 2002;133(3):373-85.
65. Jackson TL, Danis RP, Goldbaum M, et al. Retinal vascular abnormalities in neovascular age-related macular degeneration. Retina 2014;34(3):568-75.
66. Spaide RF. New proposal for the pathophysiology of type 3 neovascularization as based on multimodal imaging findings. Retina 2019;39(8):1451-64.
67. Borrelli E, Mastropasqua L, Souied E, et al. Longitudinal assessment of type 3 macular neovascularization using rhree-dimensional volume-rendering optical coherence tomography angiography. Canadian Journal of Ophthalmology 2021.

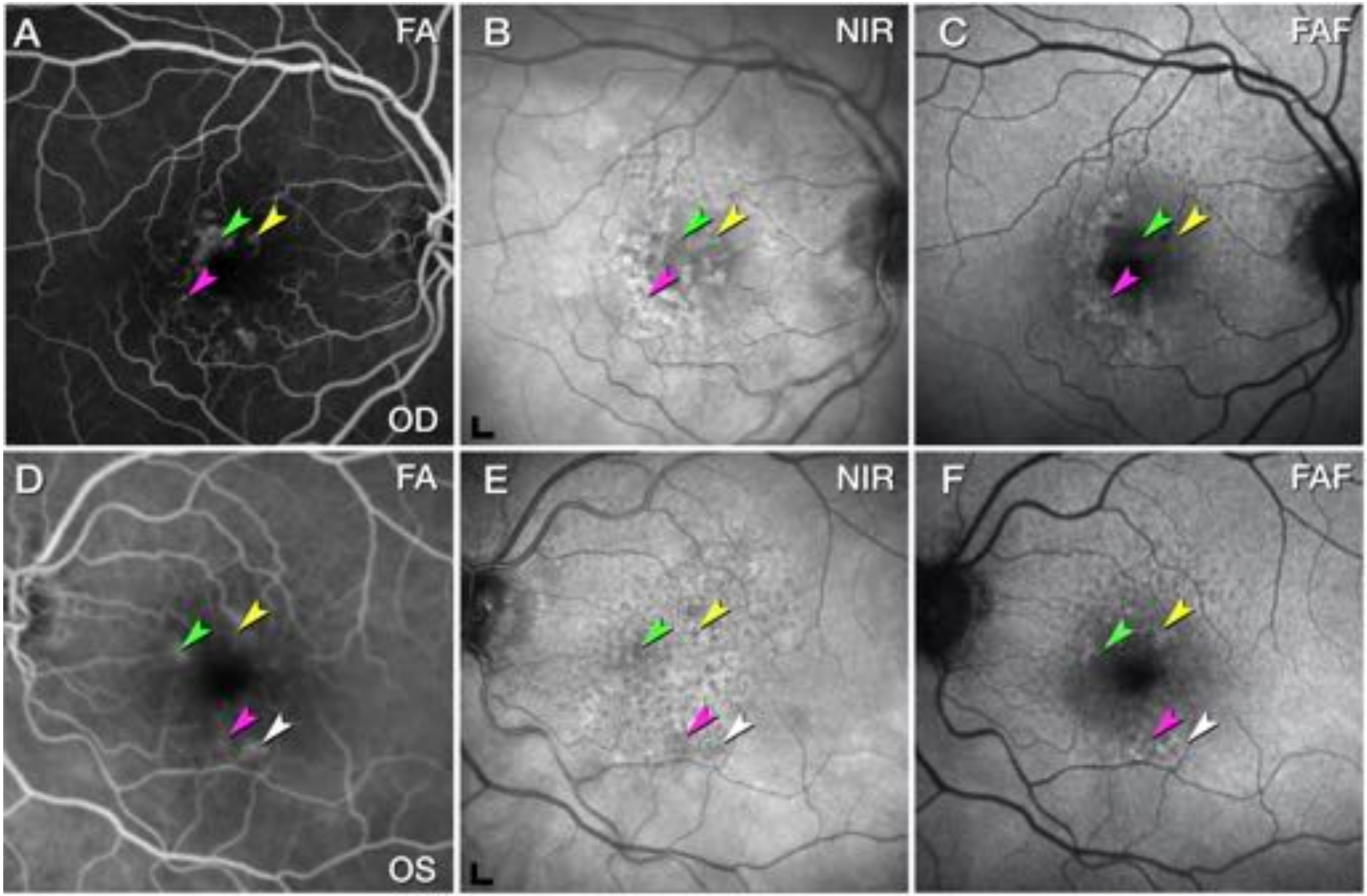
A
FA
OD
B
NIR
L
C
FAF
D
FA
OS
E
NIR
L
F
FAF

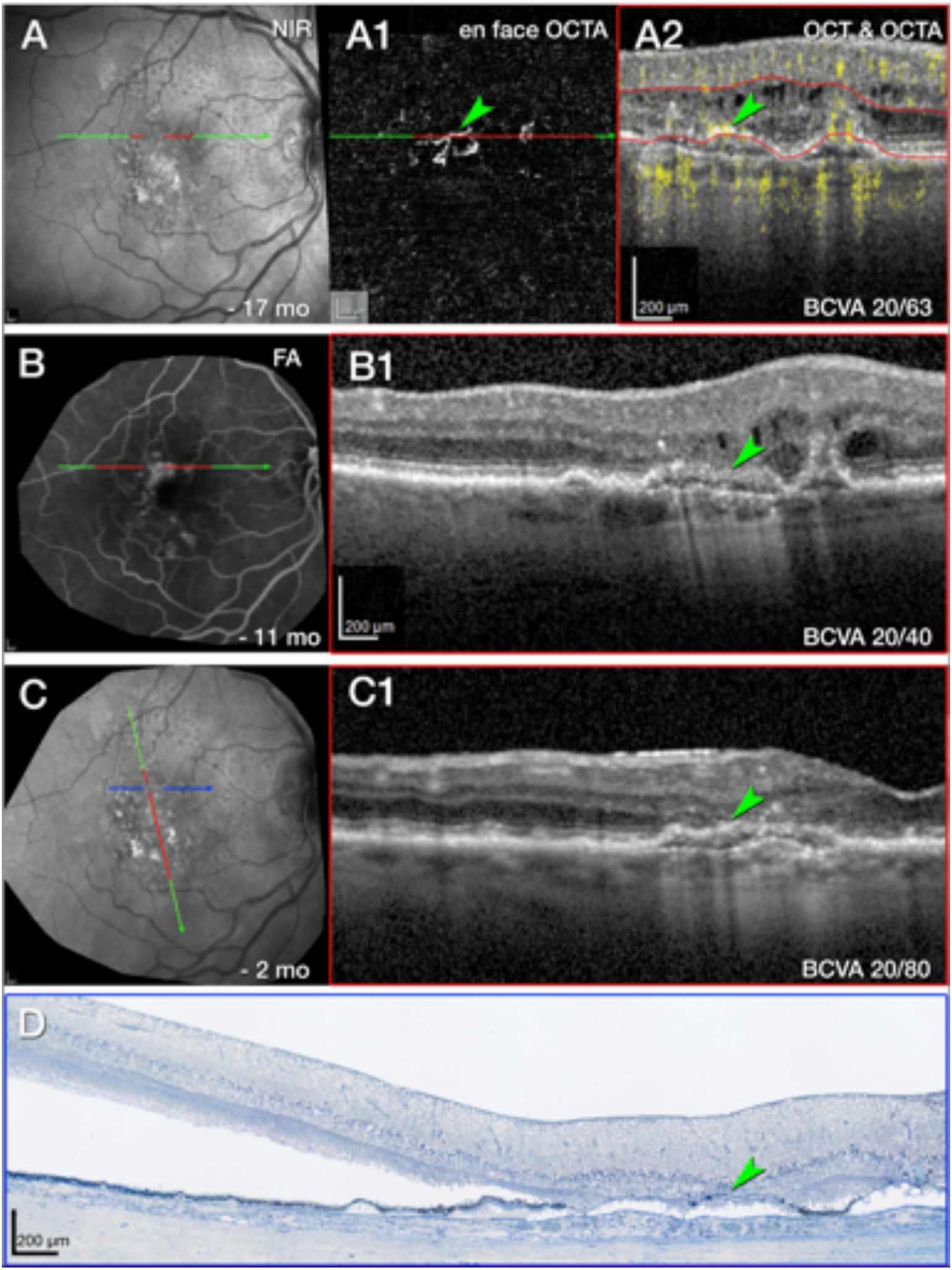
A
NIR
- 17 mo
A1
en face OCTA
A2
OCT & OCTA
200 µm
BCVA 20/63
B
FA
- 11 mo
B1
200 µm
BCVA 20/40
C
- 2 mo
C1
BCVA 20/80
D
200 µm

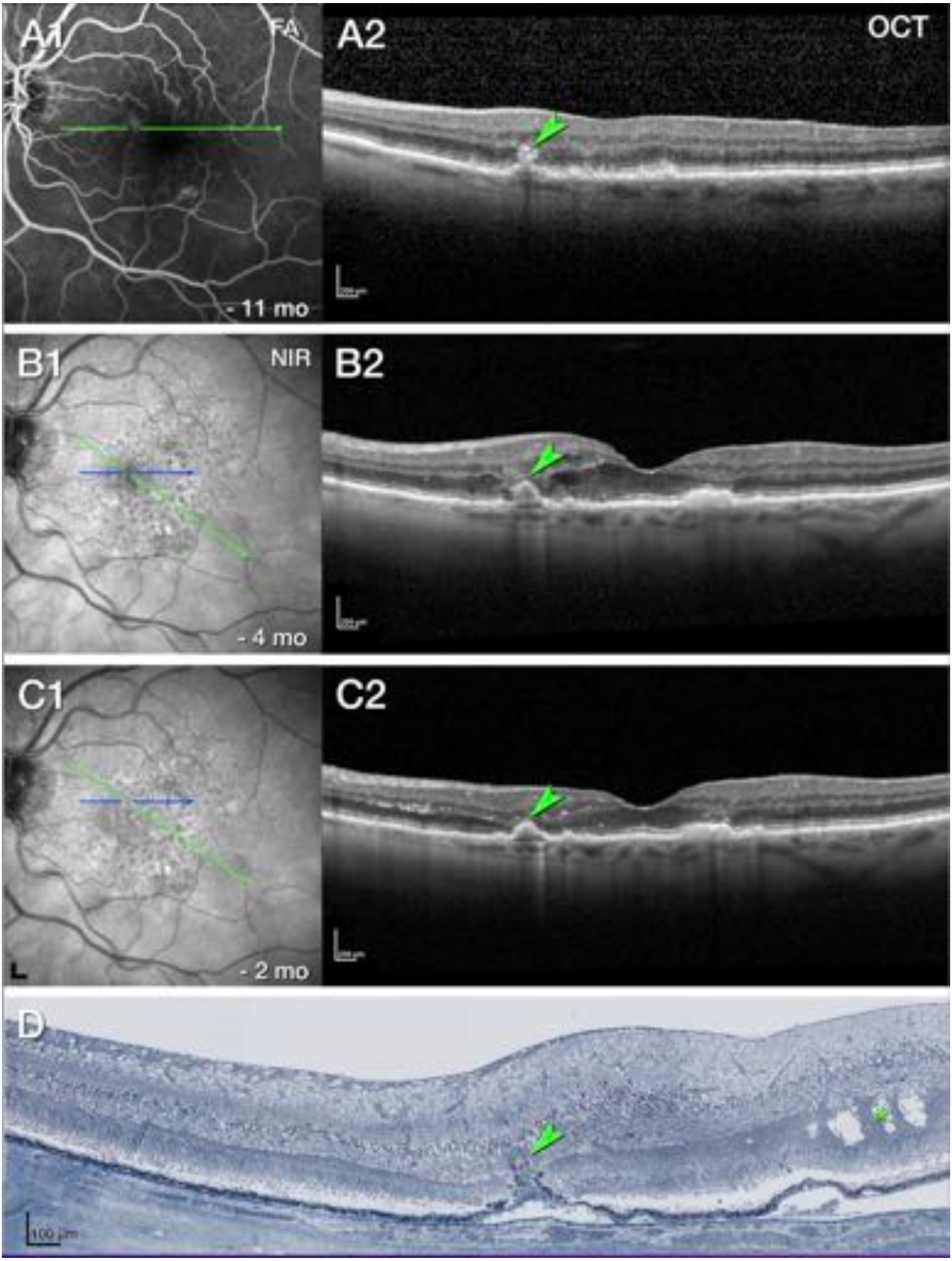
A1
FA
- 11 mo
A2
OCT
B1
NIR
- 4 mo
B2
C1
- 2 mo
C2
D
100 µm

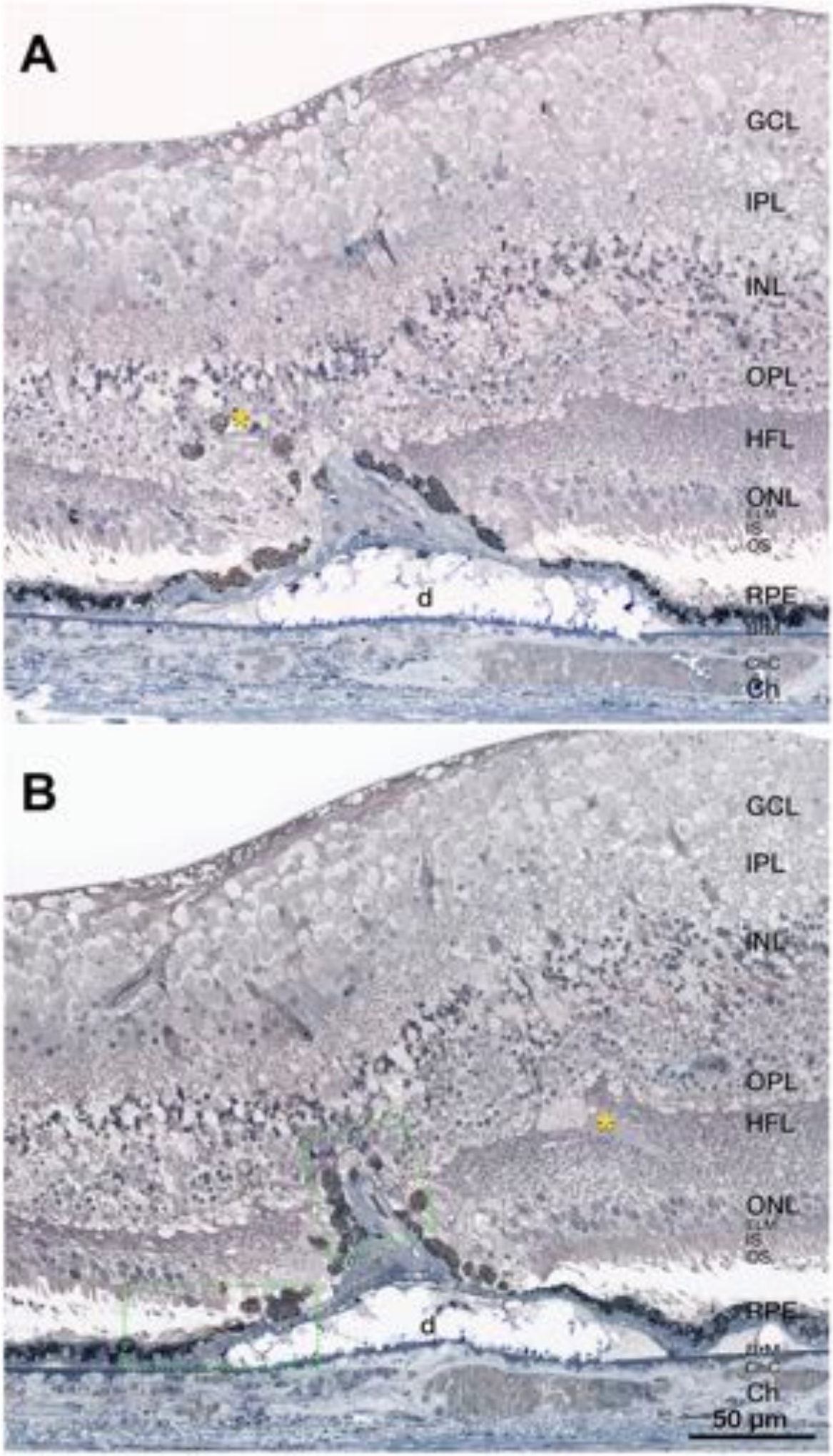
A
GCL
IPL
INL
OPL
HFL
ONL
ILM
IS
OS
d
RPE
BlM
CoC
Ch
B
GCL
IPL
INL
OPL
HFL
ONL
ILM
IS
OS
RPE
d
BlM
CoC
Ch
50 µm

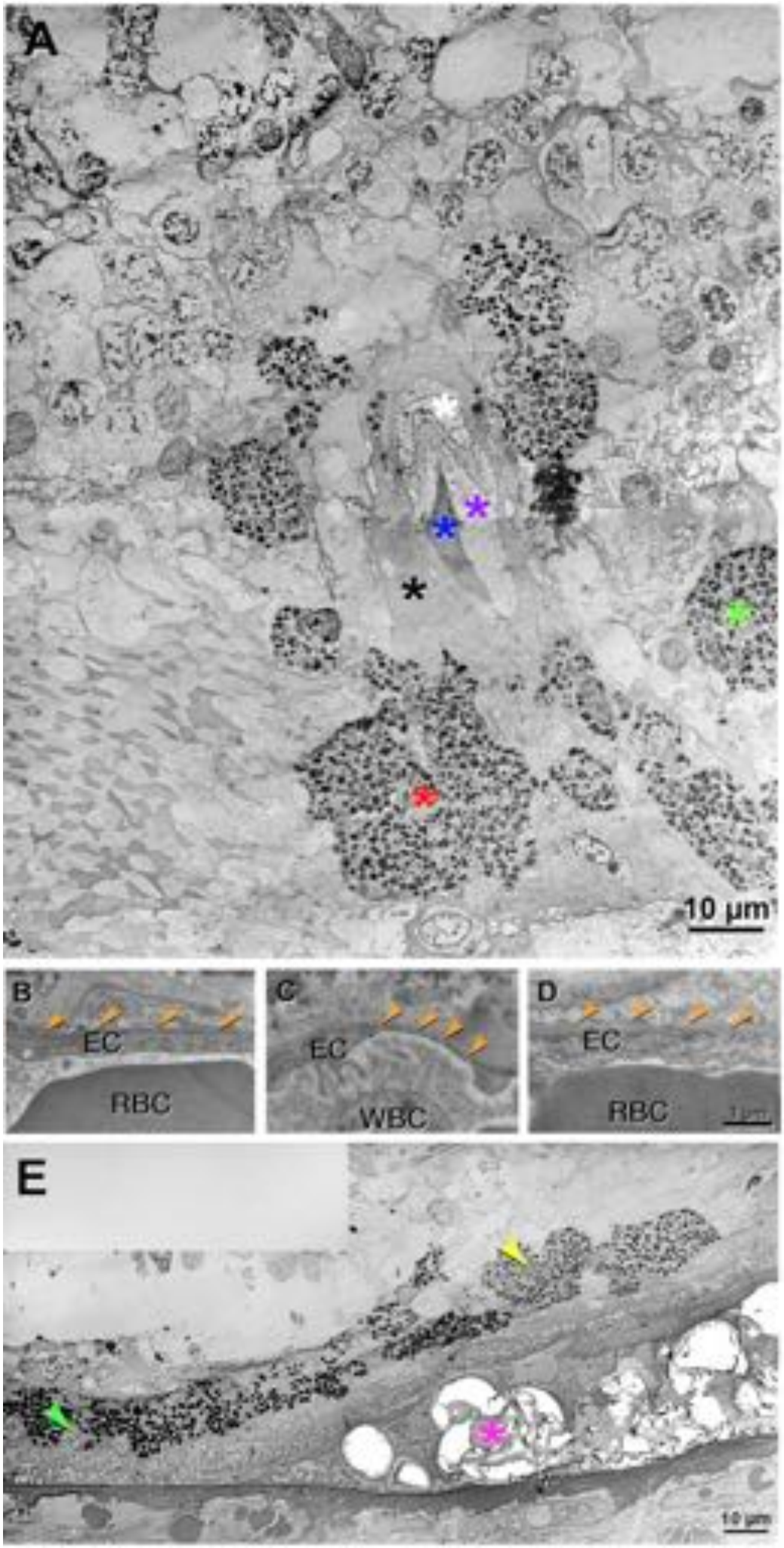
A
10 µm
B
EC
RBC
C
EC
WBC
D
EC
RBC
E
10 µm

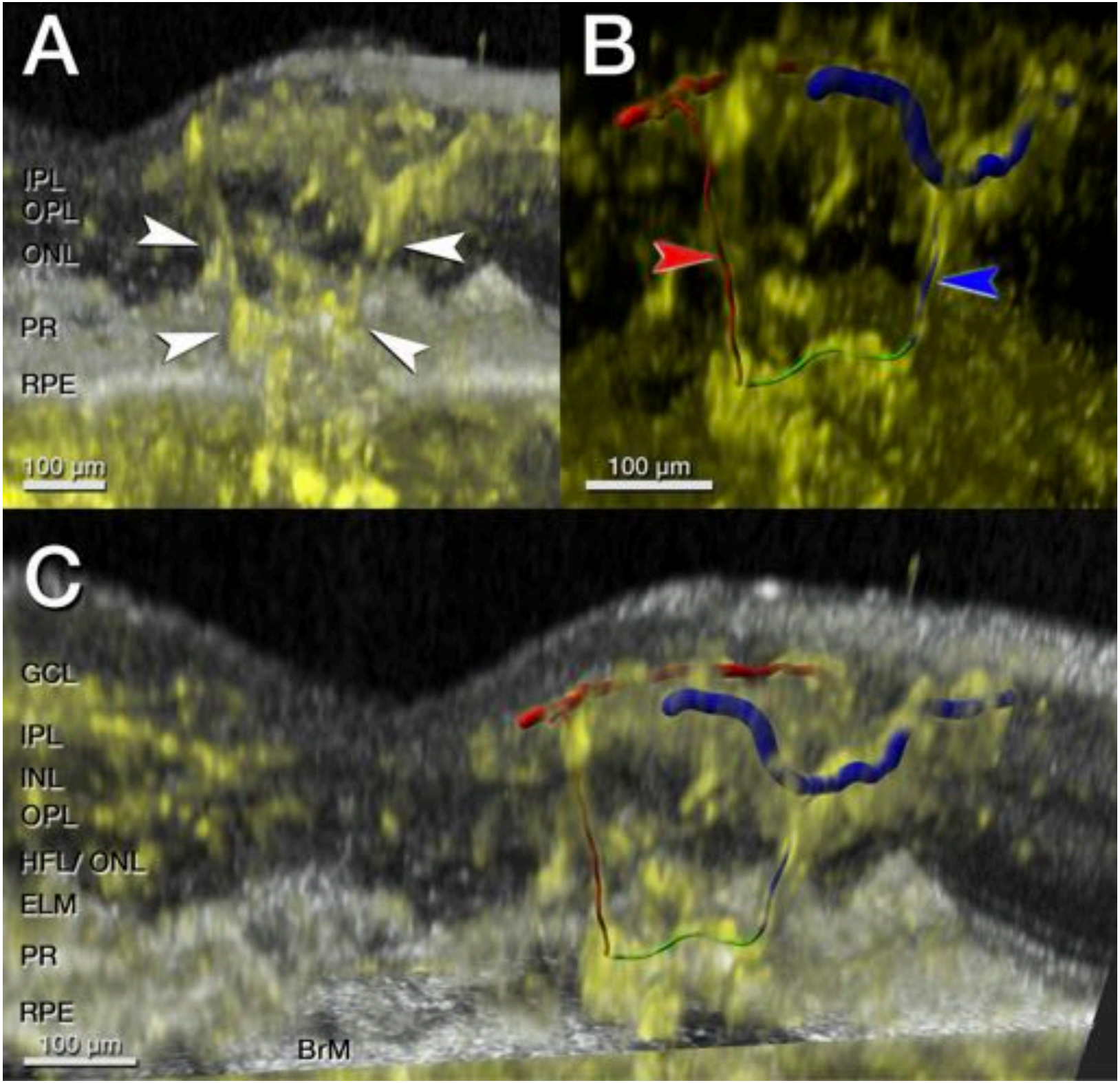
A
IPL
OPL
ONL
PR
RPE
100 µm
B
100 µm
C
GCL
IPL
INL
OPL
HFL/ ONL
ELM
PR
RPE
100 µm
BrM

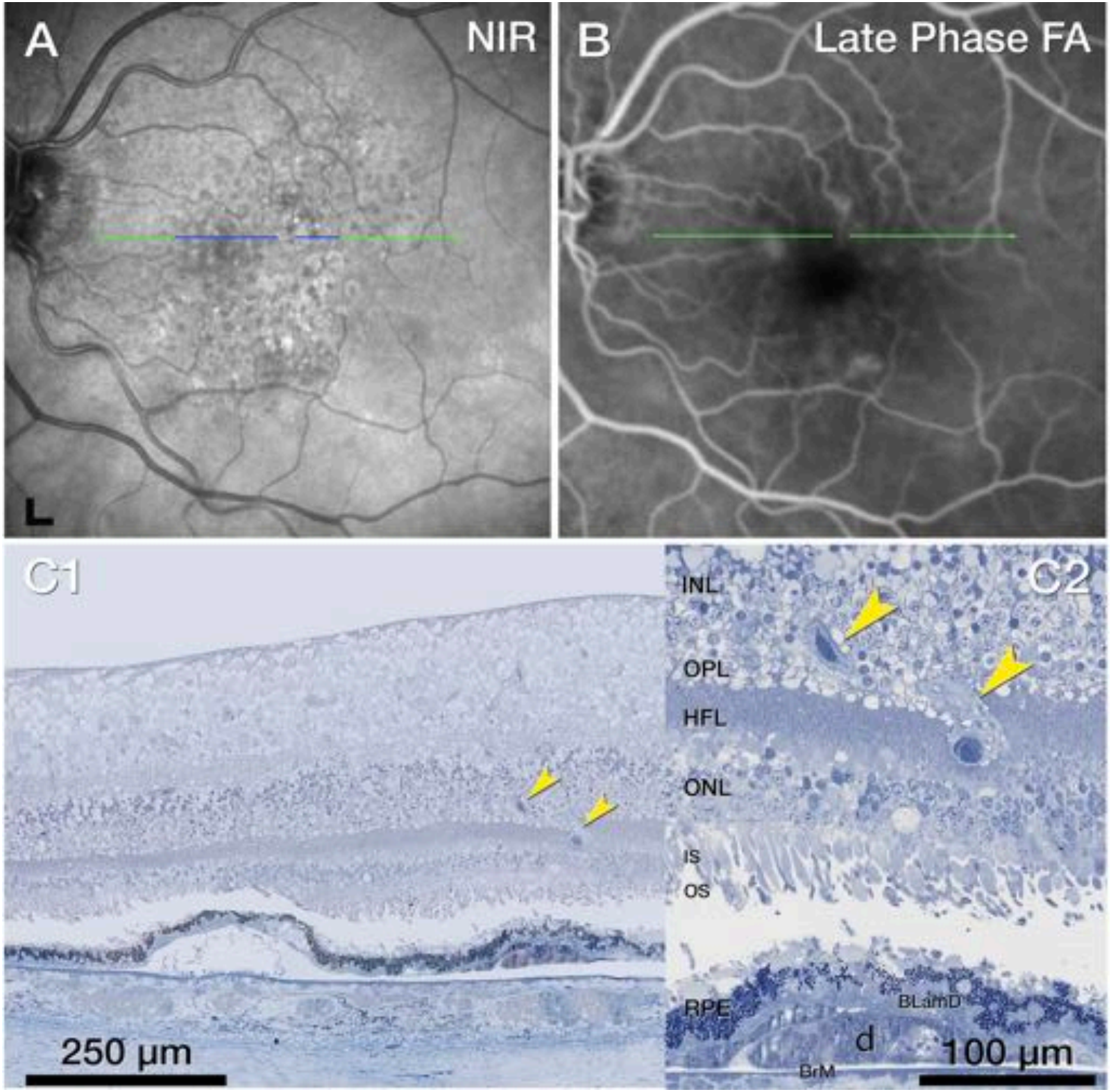
A
NIR
L
B
Late Phase FA
C1
250 µm
C2
INL
OPL
HFL
ONL
IS
OS
RPE
BLamD
d
BrM
100 µm

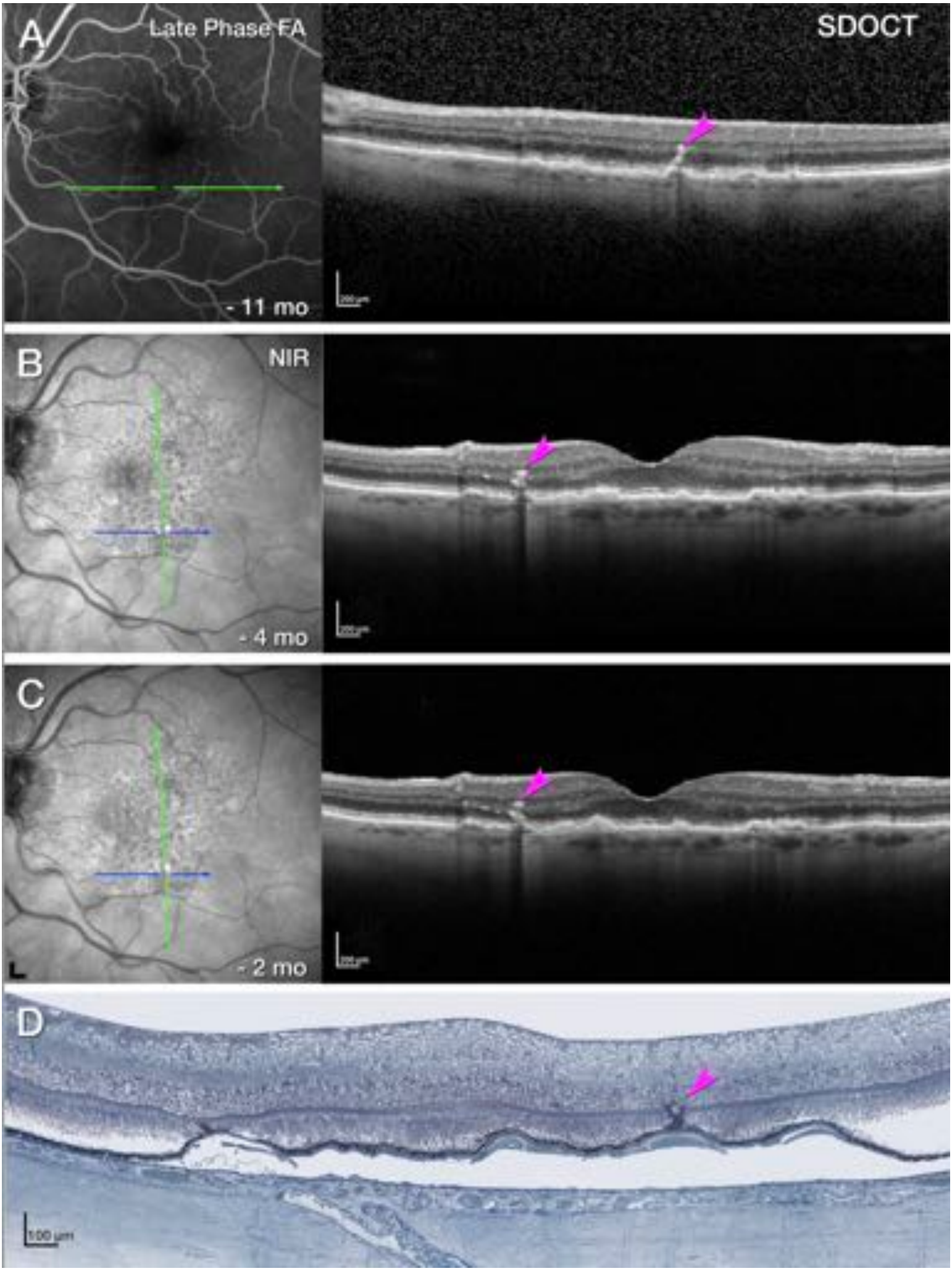
A
Late Phase FA
SDOCT
- 11 mo
B
NIR
- 4 mo
C
- 2 mo
L
D
100 µm

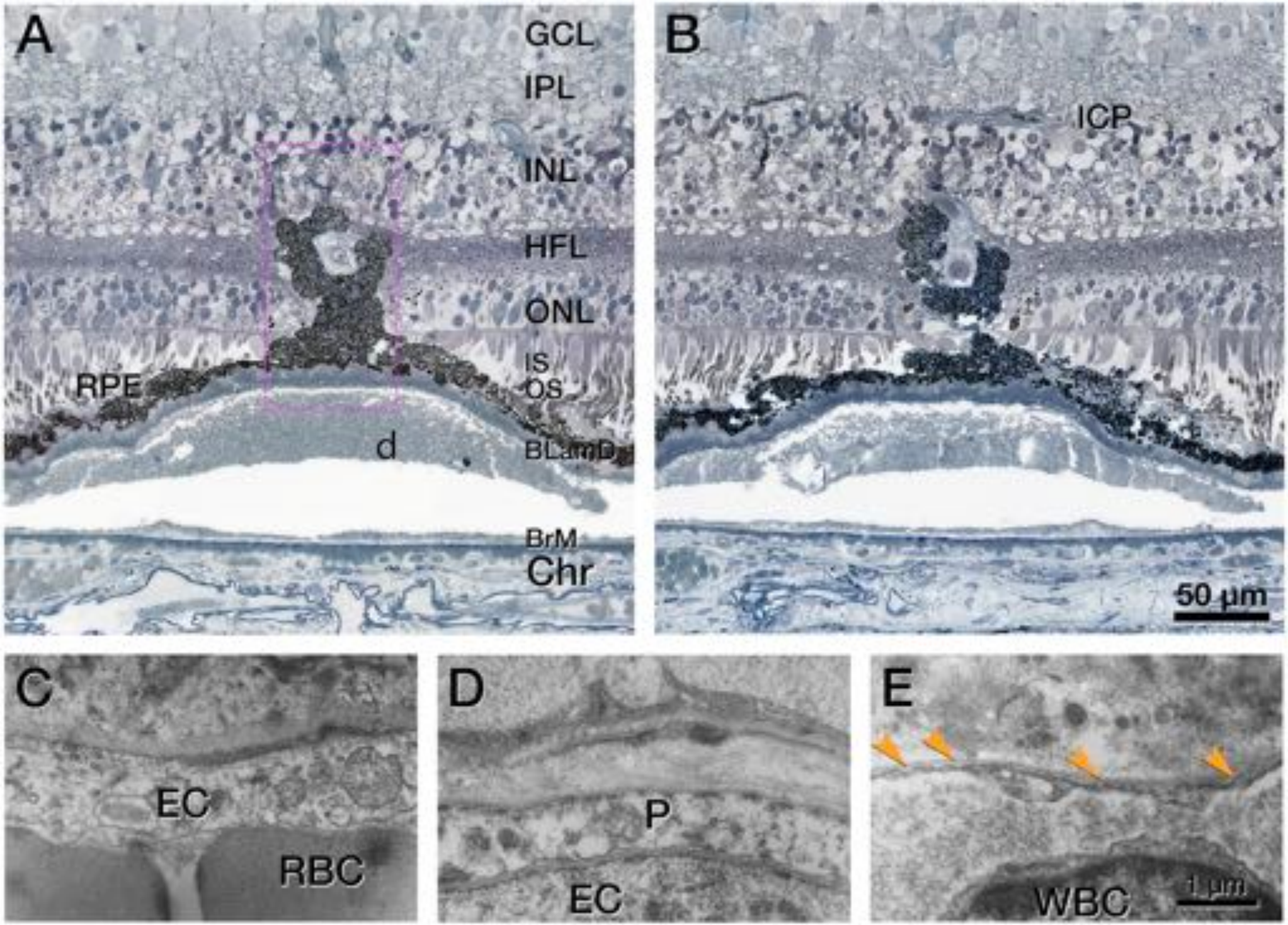
A
GCL
IPL
INL
HFL
ONL
IS
OS
RPE
d
BLamD
BrM
Chr
B
ICP
50 µm
C
EC
RBC
D
P
EC
E
WBC
1 µm

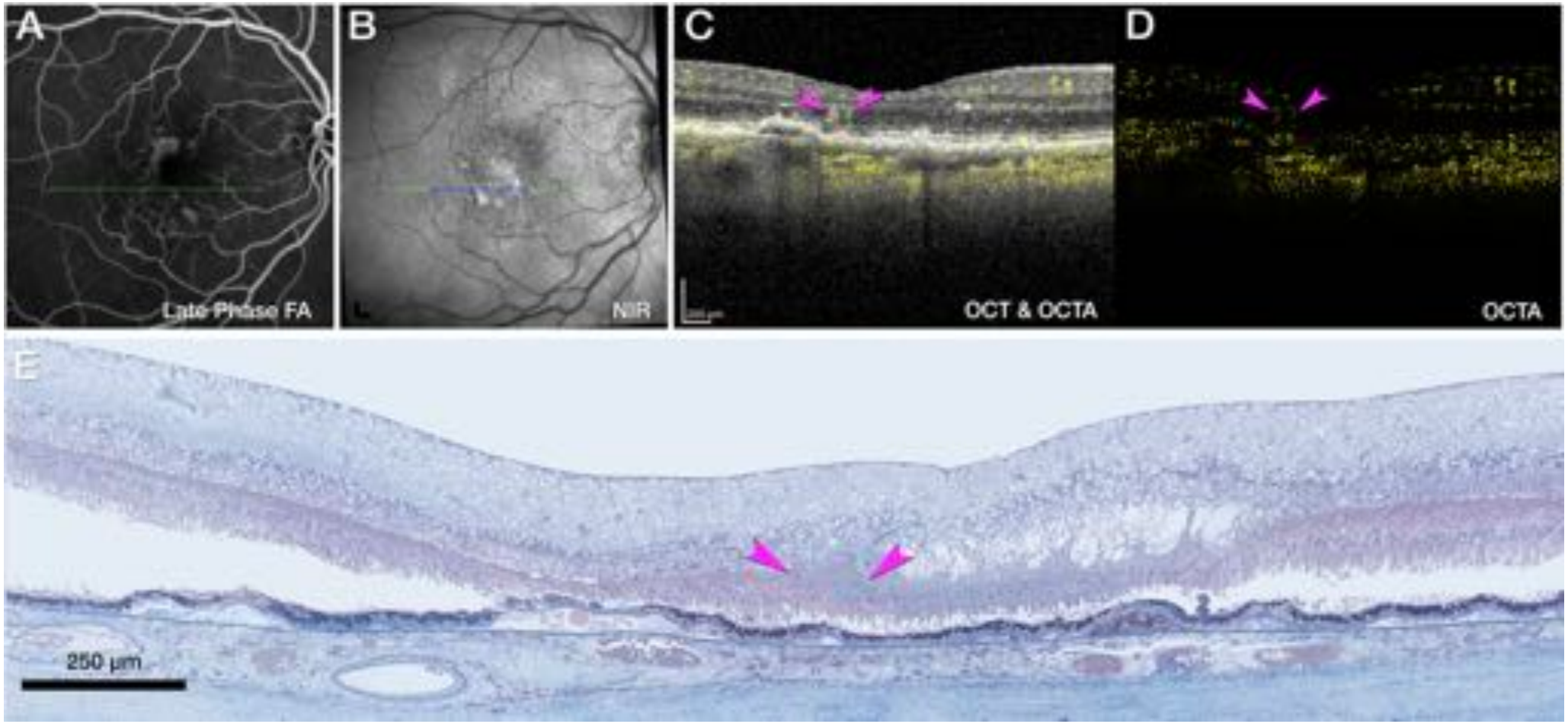
A
Late Phase FA
B
NIR
C
OCT & OCTA
D
OCTA
E
250 µm

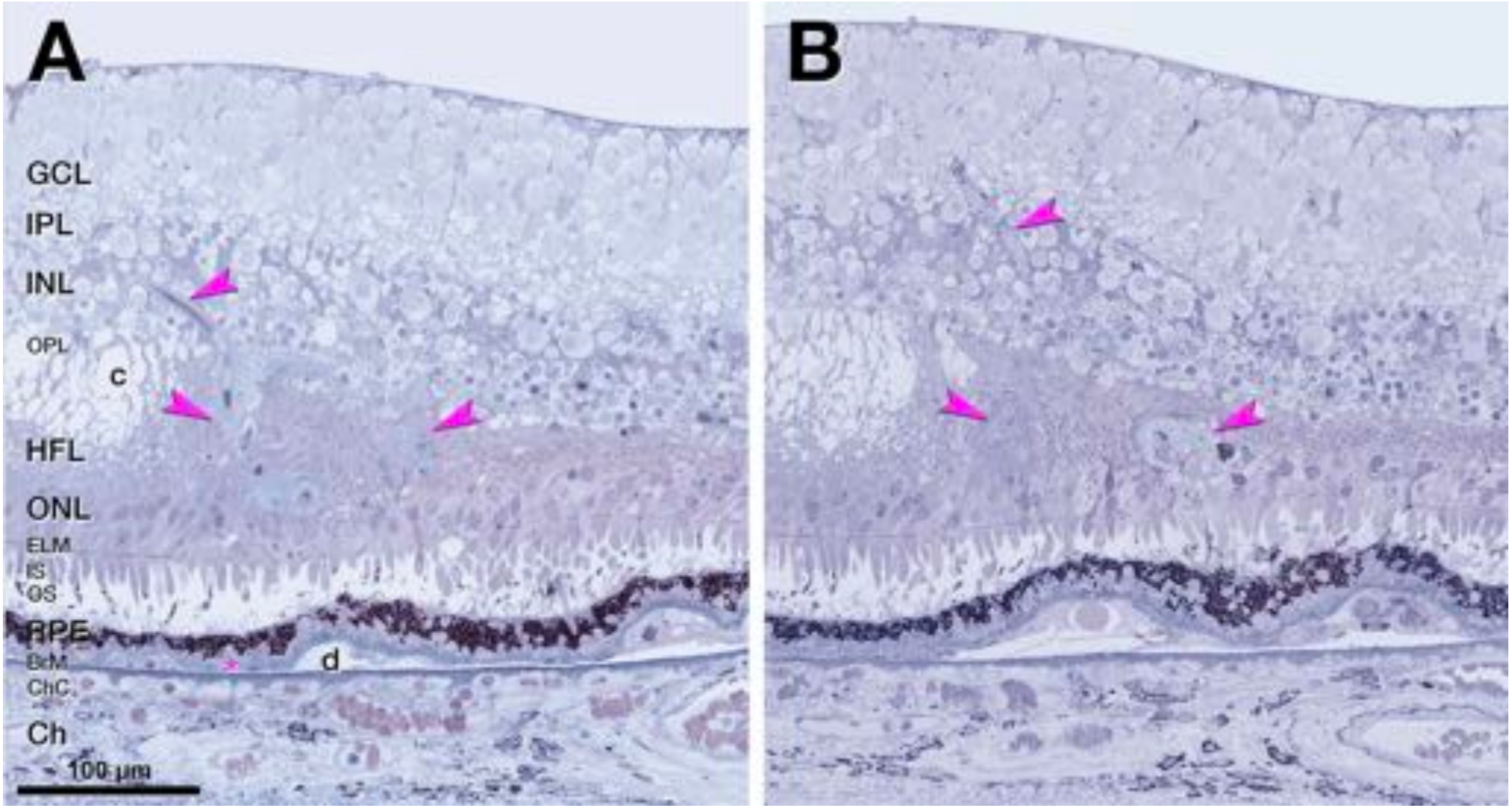
A
GCL
IPL
INL
OPL
c
HFL
ONL
ELM
IS
OS
RPE
BrM
ChC
Ch
d
100 µm
B

Table 1. Spatial distribution and vascular lesion types in treated type 3 MNV eyes.

Eye, lesion number, color in Fig. 1	Distance to fovea (µm)	ETDRS quadrants	Vortex vein quadrants	Lesion type	intravitreal anti-VEGF
OD 1 (green)	520*	S	ST	T3MNV, tangled	37
OD 2 (yellow)	1154	N	SN	T3MNV, pyramidal	37
OD 3 (fuchsia)♦	602	T	IT	Precursors or DRAMAs	37
OS 1 (yellow)	1305	S	ST	Precursor or DRAMA	6
OS 2 (white)	1520	I	IT	not found	6
OS 3 (fuchsia)	1164	I	IT	Precursor or DRAMA	6
OS 4 (green)	1101	N	ST	T3MNV, pyramidal	6

Table 1. Spatial distribution of and lesion type in treated type 3 MNV.

T3MNV, type 3 macular neovascularization; DRAMA, deep retinal age-related microvascular anomaly; n.a., not applicable; ETDRS quadrants: S, superior; I, inferior; N. nasal; T, temporal; Vortex vein quadrants: ST, superior temporal; SN, superior nasal; IN, inferior nasal; IT, inferior temporal.

Within each eye. lesions were numbered clockwise, starting at 12:00 in the ETDRS grid. Spatial distribution was documented according to quadrants in the ETDRS grid and vortex vein drainage systems. The ETDRS grid system is divided by 45° lines, resulting in 4 spatial descriptors (nasal, temporal, superior, and inferior). The vortex vein system is divided by 90° lines due to the area of blood drainage, resulting in 4 different descriptors (superior-temporal, superior-nasal, inferior-temporal, and inferior-nasal). In total 7 lesions could be identified on fluorescein angiography. Six lesions were located within 500 to 1500 µm of the fovea, corresponding to the inner ring of the ETDRS grid. One lesion was located outside the 1500 µm ring (1520 µm), corresponding to the outer ring of the ETDRS grid. In addition to vascular lesions, hyperfluorescence on fluorescein angiography due to window defects was detected, as reported elsewhere *(cite RCBR report)*. * Span width of tangled vascular lesion: 520-769 µm; ♦ pair of vascular lesions.